DTIC FILE COPY

SECURITY CLASSIFICATION OF THIS PAGE

REPORT DOCUMENTATION PAGE

Form Approved
OMB No 0704-0188

1a REPORT SECURITY CLASSIFICATION UNCLASSIFIED	1b RESTRICTIVE MARKINGS
2a SECURITY CLASSIFICATION AUTHORITY	3 DISTRIBUTION / AVAILABILITY OF REPORT
2b DECLASSIFICATION / DOWNGRADING SCHEDULE	
AD-A230 299	5 MONITORING ORGANIZATION REPORT NUMBER(S) AFOSR-TR- 91 1185
6a NAME OF PERFORMING ORGANIZATION Univ. of Arkansas for Med. Sci. NMR Laboratory	6b OFFICE SYMBOL (If applicable)
6c ADDRESS (City, State, and ZIP Code) 4301 West Markham Street Little Rock, AR 72205	7a NAME OF MONITORING ORGANIZATION
	7b ADDRESS (City, State, and ZIP Code)
8a NAME OF FUNDING / SPONSORING ORGANIZATION Air Force Office of Scientific Research	8b OFFICE SYMBOL (If applicable) AFOSR/NE
8c ADDRESS (City, State, and ZIP Code) Building 410 Bolling AFB, D.C. 20332-6448	9 PROCUREMENT INSTRUMENT IDENTIFICATION NUMBER AFOSR-89-0418
	10 SOURCE OF FUNDING NUMBERS: PROGRAM ELEMENT NO 61102F; PROJECT NO 2306; TASK NO A3; WORK UNIT ACCESSION NO

DTIC ELECTE DEC 26 1990

11 TITLE (Include Security Classification)
NMR IMAGING OF ELASTOMERIC MATERIALS

12 PERSONAL AUTHOR(S)
Komoroski, Richard Andrew; Sarkar, Subhendra N.; Wooten, E. Wrenn

13a TYPE OF REPORT	13b TIME COVERED	14 DATE OF REPORT (Year, Month, Day)	15 PAGE COUNT
Annual	FROM 89/07/01 TO 90/07/31	90/11/30	

16 SUPPLEMENTARY NOTATION

17 COSATI CODES		
FIELD	GROUP	SUB-GROUP

18 SUBJECT TERMS (Continue on reverse if necessary and identify by block number)
nuclear magnetic resonance, imaging, elastomers, tires, composites, porous, spin echo, lithium-7, fluorine-19, oil cores, interfaces, curing, filler, NMR imaging, relaxation

19 ABSTRACT (Continue on reverse if necessary and identify by block number)

NMR imaging has been applied to some elastomeric materials of industrial and military interest. The T_2 spin-spin relaxation times of common elastomers, particularly after filling and curing, are sufficiently short that spin-echo sequences at submillisecond echo times cannot produce T_2-independent images. The sensitivity to T_2 potentially makes spin echo imaging a good probe of elastomer blend composition, as demonstrated for a series of filled and cured cis-polybutadiene, styrene-butadiene rubber blends. The technique can be used to distinguish good and bad carbon black dispersion in actual tire tread samples. The configuration of polyester tire cord, voids, rubber layer boundaries, apparent migration of additives, and other inhomogeneities can be detected in end-product tire samples. NMR images have been obtained for four porous glass disks of different porosities as models of materials such as oil cores. The mottled appearance often seen for such images is attributed largely to insufficient signal-to-noise ratio, and not pore structures. Comparison of spin-echo and gradient-echo images demonstrates the defect-magnification effect of the gradient-echo

20 DISTRIBUTION / AVAILABILITY OF ABSTRACT	21 ABSTRACT SECURITY CLASSIFICATION
☑ UNCLASSIFIED/UNLIMITED ☐ SAME AS RPT ☐ DTIC USERS	UNCLASSIFIED
22a NAME OF RESPONSIBLE INDIVIDUAL	22b TELEPHONE (Include Area Code) (202) 767-4935 / 22c OFFICE SYMBOL NE

DD Form 1473, JUN 86 — Previous editions are obsolete. — SECURITY CLASSIFICATION OF THIS PAGE

NMR Imaging of Water in Model Porous Materials

SUBHENDRA N. SARKAR, E. WRENN WOOTEN* and

RICHARD A. KOMOROSKI+

Departments of Radiology and Pathology, University of Arkansas for Medical Sciences, Little Rock, AR 72205

* Current address: Department of Chemistry, University of California, Berkeley, CA 94720

+ To whom correspondence should be addressed

ABSTRACT

Nuclear magnetic resonance images have been obtained for four porous glass disks of different porosities as models of materials such as oil cores. The mottled appearance often seen for such images is attributed largely to insufficient signal-to-noise ratio, and not pore structures. Comparison of spin-echo and gradient-echo images demonstrates the defect-magnification effect of the gradient-echo sequence seen previously for elastomers. The advantages of volume imaging, isotropic voxels in thin slices, and higher resolution are demonstrated for porous materials. Images with isotropic voxels of 80-100 μm on a side were obtained in several hours. Dramatic differences are not seen at 100 μm resolution for disks of average pore size 15 to 200 μm because the images are dominated by the large-pore tail of the size distribution.

INDEX HEADINGS: NMR imaging
Porous materials
Spin relaxation

INTRODUCTION

Nuclear magnetic resonance (NMR) imaging has seen increasing use in the analysis of materials.[1] Because NMR imaging is primarily a technique for liquids, most work to date has involved imaging ^1H rich solvents in porous solids or elastomers of high molecular mobility.[2] Areas of interest have been analysis of oil cores, quality control in the processing of green ceramics, void distributions in composite materials, and solvent diffusion in polymers.

A variety of oil cores has been imaged for rock defects, porosity, water and oil distribution, and in flow studies.[3-5] Although defects such as cracks and large voids (both accessible and inaccessible to H_2O) were readily seen, the relationship of the NMR image to pore size and its distribution was not apparent because the image pixel size was typically much larger than the pore size, and the slices examined were thick (1-10 mm). The mottled appearance typical of oil core images was also observed for NMR images of homogeneous rubber,[2] where it was attributed to low signal-to-noise (S/N) ratio in combination with the signal threshold chosen for image display. Benzene soaked, partially sintered Al_2O_3 disks have been imaged without resolving individual pores.[6] These workers have also imaged 2.5% polymeric binder in Al_2O_3 green body at 330 x 330 μm in-plane resolution.[7]

We examine here several aspects of NMR imaging as they

apply to porous materials. The effect of resolution relative to the pore size is examined for sintered glass disks of various pore sizes. The value of thin slices and isotropic voxels, either in standard spin-echo (SE) or volume imaging, is demonstrated. As done previously for elastomeric materials,[2] defect magnification can be obtained using the gradient-echo (GRE) sequence.

EXPERIMENTAL SECTION

Samples: Sintered glass disks of various porosities were obtained from Kontes, Vineland, NJ. The disks were about 4 to 5 mm thick and about 6 cm in diameter. From the difference in weight when dry and when fully soaked, the approximate fraction of total volume accessible to water can be obtained. These fractions are listed in Table 1 for the case when the disks are soaked in air at atmospheric pressure. These proportions were verified approximately by the total spin echo intensities of the ^1H NMR signals from different disk samples at 4.7 T after normalizing the signals for the various spin-spin relaxation time (T_2) values assuming an exponential decay.

Imaging at 1.5 T: The whole disks were soaked in deionized water for several hours and clamped into a flat plexiglas holder fitted to the disks. Most residual water was removed, leaving a thin layer below the disks to serve as a source of water to avoid drying during imaging. A flat plate was screwed on top with an O-ring seal to minimize

evaporation.

Images were obtained at 63.9 MHz on a General Electric Signa clinical magnetic resonance imaging system with a maximum gradient strength of 1 G/cm. A 5-inch general purpose surface coil was used to provide the rf field. The entire disk was laid flat on the surface coil at several cm distance to insure reasonably homogeneous excitation. Radiofrequency field homogeneity was confirmed in one case by comparison to an image using a cylindrical coil. Typically an 8-12 cm field of view and acquisition matrix of 256 x 128 were used. A single-slice, spin-echo sequence with 1-50 excitations, time to echo (TE) of 20 ms, and pulse sequence delay (TR) between 1000-2000 ms was used to image 3 mm thick slices (the minimum on the Signa) within 4 min. to 3 hrs. Gradient-echo images with flip angles of 20-90^{o}, TE of 11-12 ms, TR of 600-1000 ms, and total imaging time of 17-35 min. were also obtained. Basic SE and GRE sequences have been described previously.[2] Three-dimensional volume images[8] using a gradient-echo sequence required about one hour to provide a set of 28 images, each for a 1 mm thick slice.

Spin-lattice relaxation time (T_1) values were measured using a standard inversion recovery sequence under the same conditions as for imaging at 1.5 T except using a TR of 15 s, six dummy scans, and a 180-90 pulse separation (TI) of 7-1600 ms. The spectra were integrated to yield intensities M(t) and the T_1s extracted from plots of $\ln[M_0-M(t)]$.

Imaging at 4.7 T: The ^1H images at 4.7 T (200.1 MHz)

were collected at a gradient strength of 20 G/cm on a General Electric Omega CSI-4.7 with an Acustar gradient system of bore size 120 mm. An SE sequence was used with 4-lobe, slice selective sinc 90^{o} and 180^{o} rf pulses, a TE of 14 ms, and a TR of 1000 ms.

Typically 7 mm x 7 mm x 5 mm pieces were cut from the above disks and presoaked in deionized water for several hours. A single-turn, 2-cm, G.E. ^{1}H surface coil was used with a homemade acrylic plastic holder permitting manual positioning of the sample to within an accuracy of 0.1 mm. The fields of view were 10.2 mm (80 μm resolution), 12.8 mm (100 μm resolution), 25.6 mm (200 μm resolution) and 51.2 mm (400 μm resolution), all with data matrix size 128 x 128. The slice thicknesses were equal to the in-plane resolution in most cases to give nominally cubic voxels. The imaging times for the extra coarse and fine disks varied between 16 min. for the most favorable case (the extra coarse disk at 400 μm resolution) to 4.5 hrs. for the 100 μm images. The medium and coarse disks, which were of lower water content, were imaged in about 9 hrs. at 80 μm resolution. The small disk pieces were wrapped in teflon tape after soaking and sealed in 10 mm NMR tubes containing a small water reservoir away from the surface coil. This minimized drying of the samples with time. Since the rf excitation of a surface coil falls off with distance, a single parallel plane was chosen at a fixed offset from the plane of the coil, and all imaging slices were chosen relative to that plane. No attempt was

made to compare absolute signal intensities among the slices thus selected. Since there was no large amount of free water trapped in the wrapped samples, related image artifacts were minimized. However, protons from the acrylic holder appeared as a wide hump, creating problems in shimming, particularly for the samples low in water content.

Spin-spin relaxation time ($T_{2)}$ measurements were performed using the nonlocalized Hahn spin-echo sequence on the entire sample. The TE was varied between 5 and 100 ms, and the total echo magnitudes plotted vs. TE and fit to a single exponential decay to give average values for T_2.

RESULTS AND DISCUSSION

A) Signal-to-Noise Ratio

Figure 1 shows the effect of S/N ratio on the NMR image of the fine disk. One excitation and a TR of 1000 ms were used in Figure 1A, where the image has the typical mottled appearance. Fifty excitations and a TR of 1500 ms were used in Figure 1B, and the image appearance is dramatically smoother. The mottling, which might be interpreted as relating to pore structure, arises from low S/N ratio coupled with a high threshold for image display. A small circular dark spot and larger diffuse regions of lower intensity near the center of the disk are barely visible in Figure 1A, but are clearly apparent in Figure 1B. The same is true of the Gibbs artifact at the top and bottom of the image, due to insufficient data sampling in the frequency encode direction.

Because it is often not possible to signal average long enough to obtain S/N comparable to Figure 1B, care must be taken in identifying small defect structures under reduced S/N conditions.

B) Relaxation Times

The bulk T_1s (at 1.5 T) and T_2s (at 4.7 T) for the disks are listed in Table 1. Both T_1 and T_2 decrease with pore size, as expected. An attempt to relate T_1 or T_2 for the set of disks to pore size using a simple model[9] was not successful, apparently due to different pore geometries or distributions for the various disks. Images of the extra coarse disk taken at 1.5 T as a function of TR and TE did not reveal any major regional variations of T_1 or T_2 in the slice taken.

C) Spin Echo vs. Gradient Echo Images

In GRE images, the rephasing is done by reversal of the read gradient instead of applying a 180^{o} pulse as for the SE sequence. Unlike for SE images, magnetic field inhomogeneities and chemical shift effects are not refocussed at the echo maximum for GRE images. The intensities in GRE images are determined by T_2^*, the time constant for decay of the FID, and are highly sensitive to differences in magnetic susceptibility of various regions in the sample. Comparative images (Figure 2) were taken with the SE and GRE sequences at 1.5 T for the extra coarse disk. Numerous defects are observed in the spin-echo image (Figure 2A), and the central

region appears slightly darker due to a lower local concentration of H_2O. The largest defects in the SE image are interesting in that adjacent to them are bright spots from large, water-filled pores. Considerable detail is seen in the GRE image of the same slice (Figure 2B). The central region is now substantially darker than the outer region, indicating a reduced T_2^* for the central region. Many more "defects" are clearly seen, even against the mottled background, and the ones seen in the SE image appear enlarged in the GRE image. However, the bright spots near the largest defects are not apparent in the GRE image.

The results of Figure 2 are similar to those previously obtained for pure elastomers.[2] The detail in the GRE image for the most part cannot be due to T_2 effects or to direct absence of spin density because these would also be reflected in the spin-echo image. The detail probably arises from magnetic susceptibility variations near void or solid glass particle surfaces, or in regions of differing pore size or density. Hence water near the surface of a defect will have a shorter T_2^* than more distant H_2O. In a gradient-echo image these surface regions would appear darker, enlarging the apparent size of the defect.[2] Thus the water giving rise to the bright spots of Figure 2A has short T_2^* by virtue of its proximity to defects, and appears dark on the GRE image. Such an effect is observed at tissue-air boundaries in medical imaging using gradient-echo sequences.[10]

D) Volume Imaging

Multislice SE and GRE techniques are commonly used in medical applications of NMR imaging. However, the minimum slice thickness is limited by the gradient strength, and time-costly interleaving is required if contiguous slices are desired. Although contiguous slices often are not necessary for medical applications, they are very important for materials applications such as oil core profiling.[5] Three-dimensional volume imaging[11] yields thin, contiguous slices, although currently data acquisition and processing can be time-consuming, at least by medical imaging standards. Such time constraints are not as critical in NMR imaging of materials.

Figure 3 shows a basic 3D imaging sequence using a gradient echo. A thick slab is first excited in the material by simultaneously applying an rf pulse and weak slice-select gradient. Slice selection is performed by stepping a phase-encoding gradient in the slice-select direction. The number of slices is given by the number of slice-select phase encode steps, and the slice thickness is given by the field of view in that direction divided by the number of steps. The technique has been demonstrated for elastomers.[12]

Figure 4 shows two typical 1-mm thick slices from a 3D volume set at 1.5 T for the extra coarse disk. Figure 4A shows clearly the presence of numerous, well defined defects in that slice. Because of the thinner slice, defects are more well defined in a slice from the 3D dataset. Figure 4B

is taken from the same region encompassed by the 3-mm GRE slice of Figure 2B. For the large feature at the top and center of the disk, one of the bright spots seen on the SE image (Figure 2A), but not on the thicker-slice GRE image (Figure 2B), is now apparent.

E) Higher Gradient Strength and Resolution

Considerable effort is being expended in developing NMR imaging techniques applicable at the microscopic level.[13,14] Microscopic NMR imaging is expected to play a significant role for materials.[1] The primary instrumental requirement for increased resolution is powerful gradients. The resolution Δx in an NMR image is given by

$$\Delta x = 1/(\gamma \cdot G \cdot AT) \qquad (1)$$

where γ is the magnetogyric ratio, G is the gradient strength, and AT is the data acquisition time. Figure 5 shows plots of G *vs.* AT for various image resolutions. The significance of the acquisition time is that in echo imaging, it is limited by (and often equal to) the echo time TE. For materials, T_2 can be quite short, and hence TE or AT cannot be lengthened without loss of echo signal.

Another consideration is the resonance line width for the material. The spread of frequencies ($\gamma G \Delta x$) caused by the gradient must be larger than the spread inherent in the line width $\Delta\nu_{1/2}$. This relationship, which is just a different way of expressing Eq. 1, is also shown in Figure 5. The relatively large line widths seen for materials also necessitate powerful gradients. At 4.7 T our line widths

were about 250 Hz (fine and extra coarse disks) and 500 Hz (medium and coarse disks), which puts a resolution limit of 35-50 μm at 20 G/cm for these materials.

To date, most NMR imaging of materials has been with highly anisotropic voxels and very poor resolution perpendicular to the slice. The advantage of isotropic voxels for visualizing complex 3D structures and minimizing confusing partial volume effects has been recognized.[15] Although 3D volume imaging may ultimately be the method of choice for obtaining isotropic voxels, it is possible to use the single-slice technique at moderately good resolution. Figures 6A-C show images (4.7 T, 20 G/cm) of a 7x7 mm piece of the extra coarse disk at three different isotropic resolutions--less than, at, and greater than the nominal pore size. As expected, the images are dramatically different and, in particular, display how features in the low resolution image arise from different planes in the slice. In the 100-μm isotropic-voxel image, there are a few small and intense spots whose size is about 190 μm x 190 μm in plane and are either single pores or collections of smaller pores. Longer spots may be pores connected in plane. Small and weak spots may be from pores of about 100-μm size or less and fully included in the slice, or from larger pores partially cut by the 100-μm slice. For the 200-μm and 400-μm isotropic resolution images (Figures 6B and 6C, respectively), a few intense spots become larger as the resolution becomes coarser. Some of the spots remain bright,

implying perhaps collections of water-filled pores from various planes. The extra coarse disk seems to be very heterogeneous in pore size and connectivity.

The higher-resolution appearance of Figure 6A is retained to a large extent in Figure 6D, an image with 100 x 100 x 2000 μm voxels, even though features from the equivalent of 20,100-μm slice thicknesses contribute to the latter image. This arises from the fact that the majority of the object volume is occupied by glass, and hence a relatively large number of the anisotropic voxels has little or no signal. For porous materials of low-to-medium porosity, thick slices may provide more useful information than for relatively homogeneous materials such as polymers.

The results of Figure 6 also demonstrate that obtaining isotropic voxels at high resolution will not exact too severe a penalty in S/N ratio for porous materials. Although the voxel volume in the 100-μm image is 1/64th that of the 400-μm image, it took only 16 times (4x S/N penalty) as long to obtain the 100-μm image. This arises from the "dilution" of the signal by glass as the resolution becomes coarser.

Figure 7 shows images of portions of all the disks at 4.7 T under comparable conditions and with isotropic voxels at moderate resolution. The image of the fine disk (Figure 7D) has a more homogeneous distribution of intensities than the other disks. The sizes of the spots are not more than 160 μm and obviously not less than 100 μm. We are observing either many fine pores or the tail of a pore size

distribution containing at most 160-μm pores, or both. The images of the other three disks are in general similar in appearance among themselves. For the medium and coarse disks, the appearance is strongly influenced by the low S/N ratio. However, the lack of dramatic difference at 100-μm resolution suggests that the role of pores smaller than the pixel size is ambiguous. If the distribution of pores is homogeneous at an intermediate spatial scale (100-1000 μm) in the first three disks, then the image is probably dominated by the large-pore tail of the distribution.

The above images were obtained in signal averaging times of up to about 4 hrs. With additional signal averaging, usable images of lower S/N ratio could be obtained for isotropic voxels of 40 μm for the extra coarse and fine disks under our conditions.

CONCLUSIONS

The results presented here demonstrate the following:

(1) The mottled appearance of images of porous materials can be due to inadequate S/N;

(2) Images of 80 μm resolution can be observed by SE imaging in a few hours at 17-40% H_2O;

(3) GRE imaging can provide a magnification effect for defects in porous materials;

(4) Isotropic voxels at moderately high resolution yield superior images for porous materials with only a modest S/N penalty;

(5) The NMR images of materials with wide porosity distributions may appear similar because they are dominated by the large-pore tail of the distribution.

ACKNOWLEDGMENTS

We thank Prof. Bill Ritchey for suggesting the sintered glass disks as models. This research was funded by grant AFOSR-89-0418 from the Air Force Office of Scientific Research.

REFERENCES

1. J. M. Listerud, S. W. Sinton, and G. P. Drobny, Anal. Chem. 61, 23A (1989).
2. C. Chang and R. A. Komoroski, Macromolecules 22, 600 (1989).
3. W. A. Edelstein, H. J. Vinegar, P. N. Tutunjian, P. E. Roemer, and O. M. Mueller, SPE Preprint 18272, 101 (1988).
4. B. A. Baldwin and W. S. Yamanashi, Magn. Reson. Imaging 6, 493 (1988).
5. J. J. Dechter, R. A. Komoroski, and S. Ramaprasad, Proc. Soc. Core Analysts, #8903 (1989).
6. W. A. Ellingson, P. S. Wong, S. L. Dieckman, J. L. Ackerman and L. Garrido., Cer. Bull. 68, 1180 (1989).
7. L. Garrido, J. L. Ackerman, and W. A. Ellingson, J. Magn. Reson. 88, 340 (1990).
8. P. G. Morris, Nuclear Magnetic Resonance Imaging in Medicine and Biology (Clarendon Press, Oxford, 1986).
9. D. P. Gallegos, K. Munn, D. M. Smith, and D. L. Stermer, J. Colloid Interface Sci. 119, 127 (1987).
10. E. M. Haacke and E. M. Bellon, in Magnetic Resonance Imaging, D. D. Stark and W. G. Bradley, Eds. (C. V. Mosby., St. Louis, 1988), Ch. 8, p. 138.
11. F. W. Wehrli, op. cit., Ch. 1, p. 3.

12. C. Chang and R. A. Komoroski, in Solid State NMR of Polymers, L. R. Mathias, Ed. (Plenum, New York, 1990), in press.

13. C. D. Eccles and P. T. Callaghan, J. Magn. Reson. 68, 393 (1986).

14. J. B. Aguayo, S. J. Blackband, J. Schoeniger, M. A. Mattingly, and M. Hintermann, Nature (London) 322, 190 (1986).

15. X. Zhou, C. S. Potter, P. C. Lauterbur, and B. Voth, Abstracts, Eighth Annual Meeting., Soc. Magn. Reson. Med., 286, (1989).

FIGURE LEGENDS

Figure 1 Spin-echo NMR images of the fine porosity disk at 1.5 T. A) 1 excitation and TR of 1000 ms; B) 50 excitations and TR of 1500 ms. The faint arcs at left and bottom right in both images are due to inadequacies of photography on our Signa system and do not involve the image itself.

Figure 2 A) Spin-echo image (TE=20 ms) of a 3-mm slice through the extra coarse disk at 1.5 T; B) gradient-echo image (TE = 15 ms) of the same slice. Field of view, 8 cm; matrix size, 128 x 256; TR, 1 sec; no. of acquisitions, 8; tip angle, 20^{o}.

Figure 3 A basic 3D, GRE imaging sequence similar to that used to acquire the images in Figure 4.

Figure 4 Two, 1-mm thick slices from a 3D, GRE dataset (28 total slices) of the extra coarse disk at 1.5 T.; TR, 800 ms; TE, 20 ms; tip angle, 60^{o}; FOV, 8 cm; matrix size, 128 x 256; 1 acquisition.

Figure 5 Plots of G *vs.* AT (TE) or line width for various resolution values in NMR imaging.

Figure 6 NMR images at 4.7 T of a 7 x 7 mm portion of the extra coarse disk at three isotropic resolutions: A) 100 μm; B) 200 μm; and C) 400 μm; D) 100 x 100 x 2000 μm voxels. To the bottom and right of the images are intensity profiles of the object at the position of the parallel line on the image display.

Figure 7 NMR images at 4.7 T of portions of the A) extra coarse (100 μm), B) coarse (80 μm), C) medium (80 μm), and D) fine (100 μm) disks.

TABLE 1: Pore sizes, water contents, and spin relaxation times for porous disks.

System	Nominal Pore Size (μm)	Vol % H_2O Saturated	T_1 (ms) at 1.5 T	T_2 (ms) at 4.7 T
Pure water	---	--	2700	--
Extra coarse disk	170-220	35	2300	64
Coarse disk	40-60	20	----	56
Medium disk	10-15	24	----	39
Fine disk	4-5.5	40	2100	33

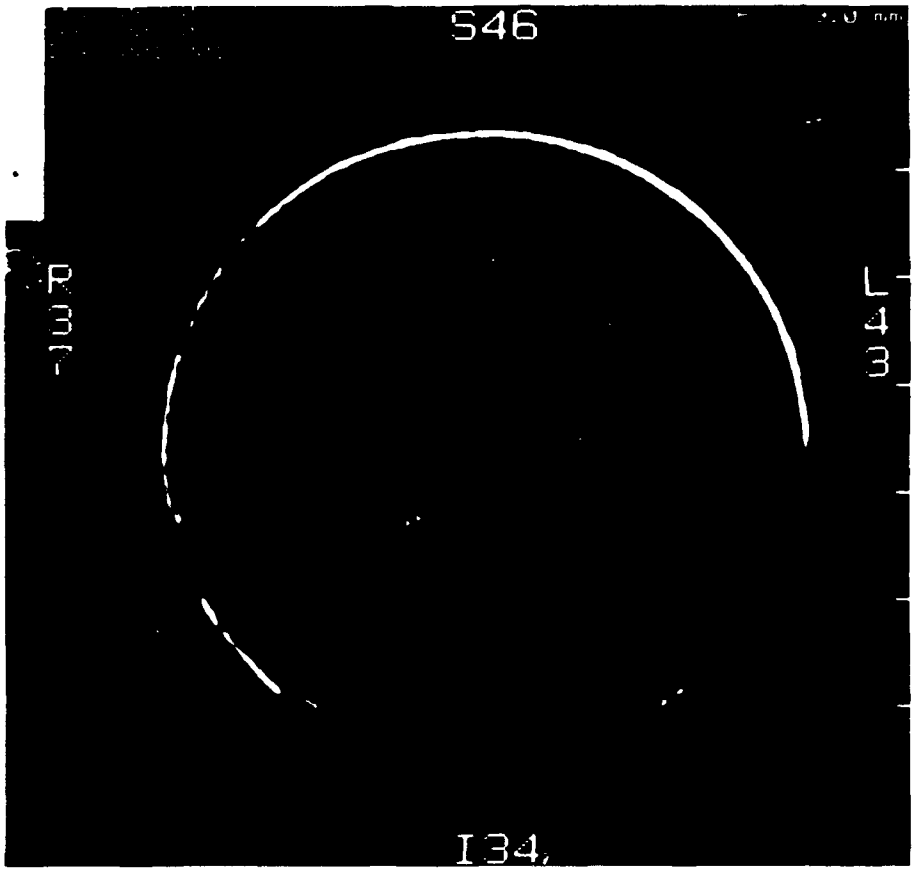
546
134

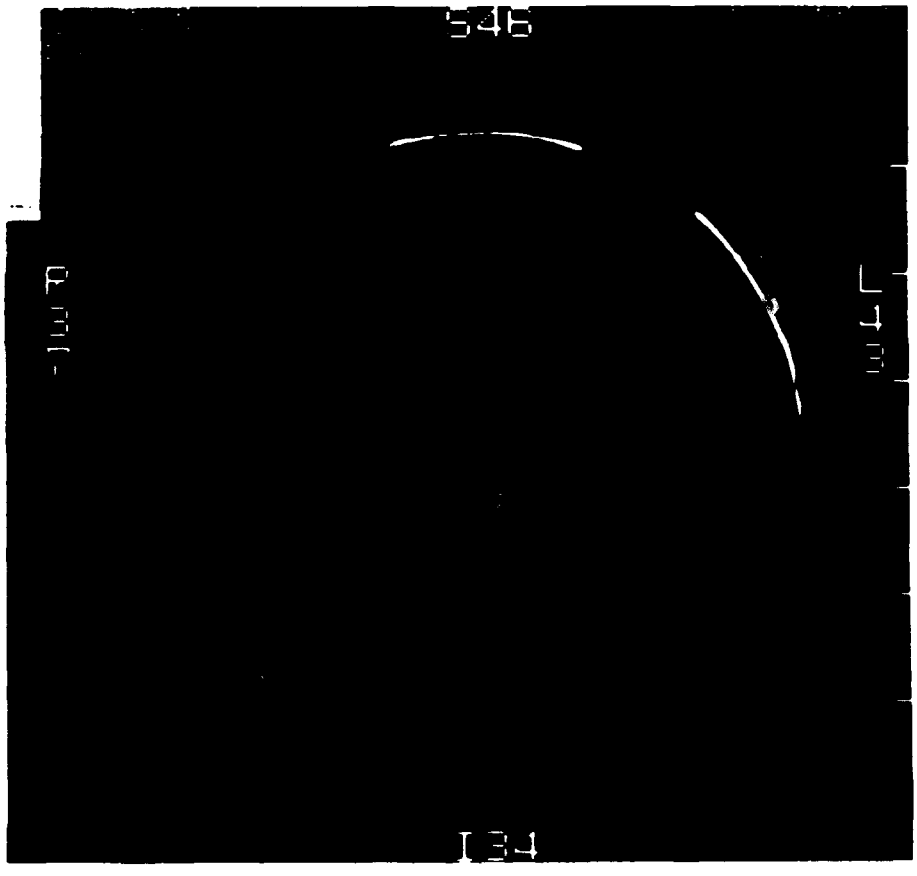
546
134

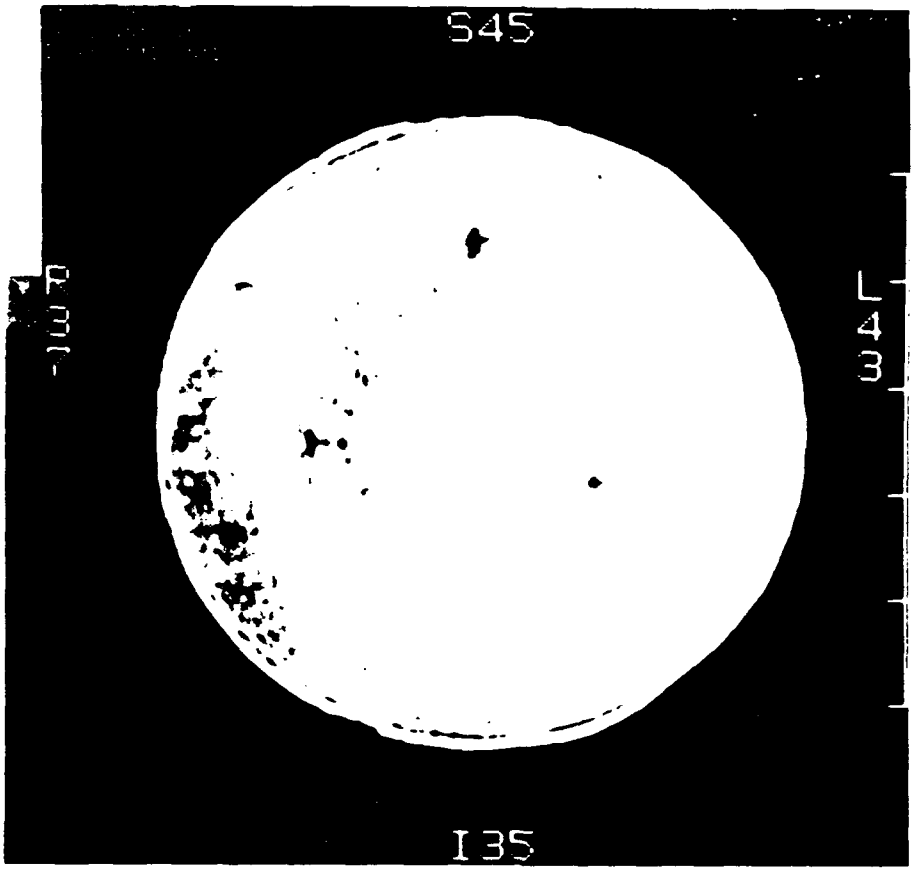
S45
I35

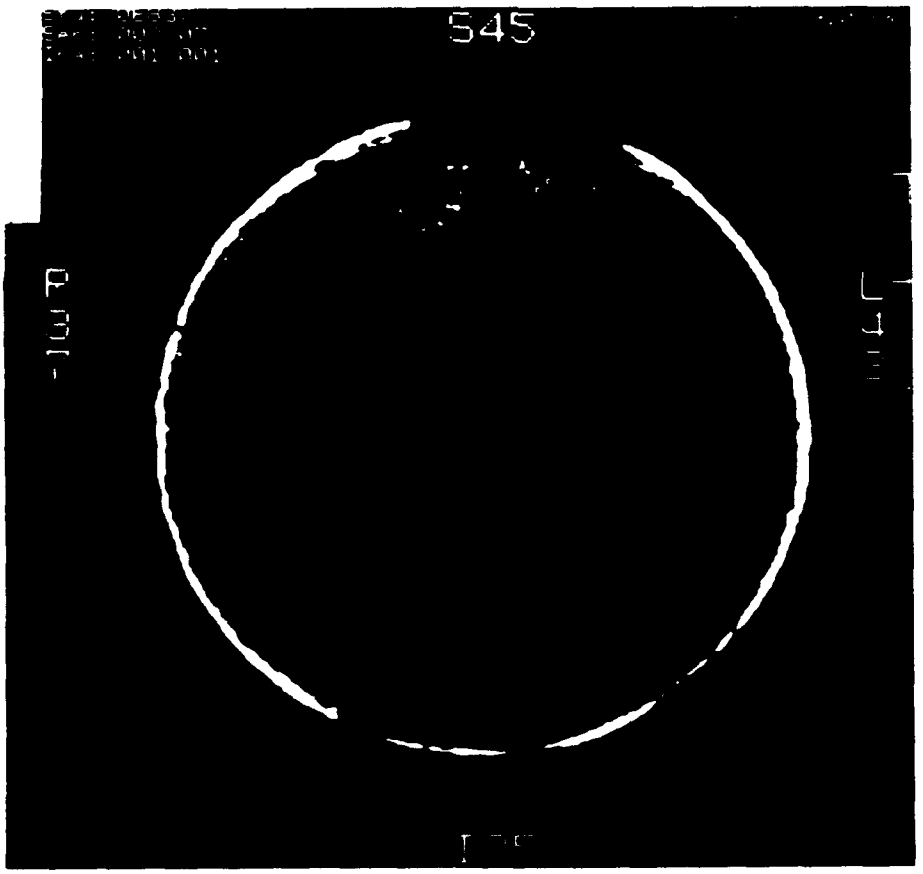
S45

Fig. 2

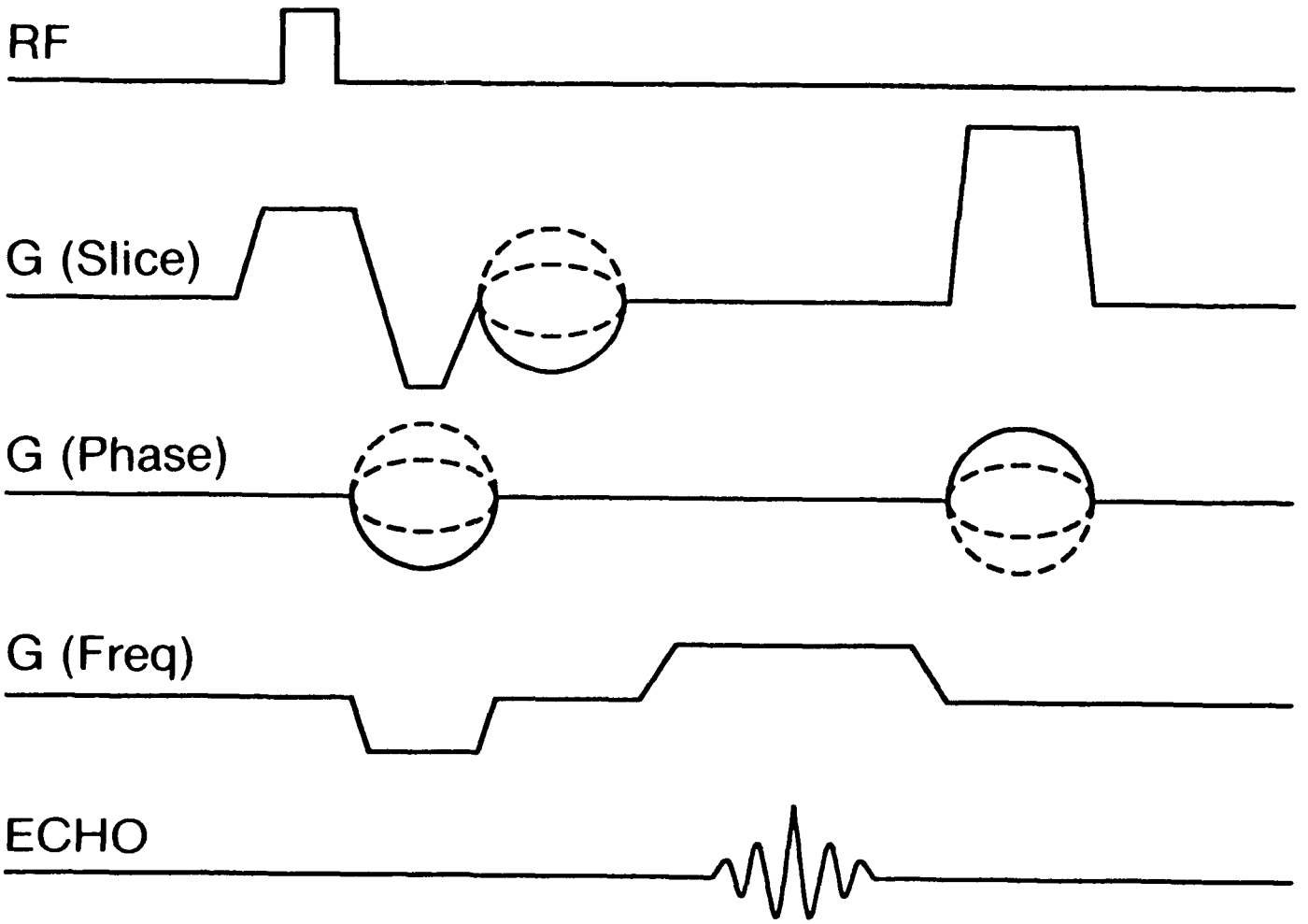

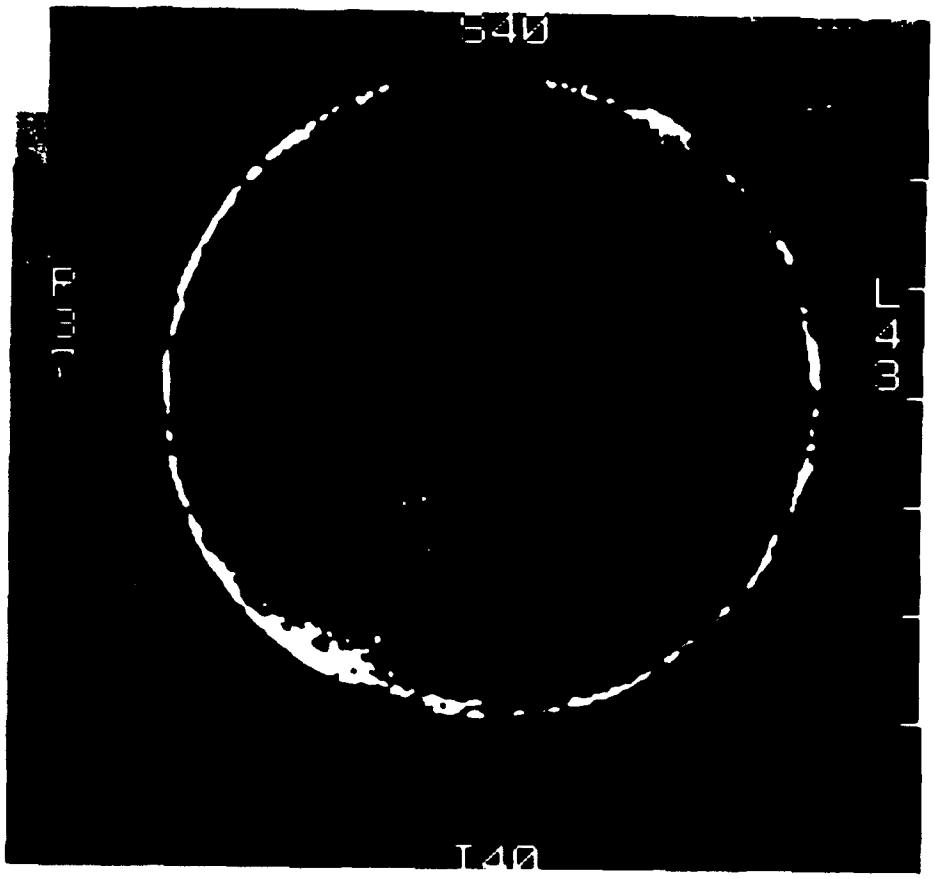
S40
I40

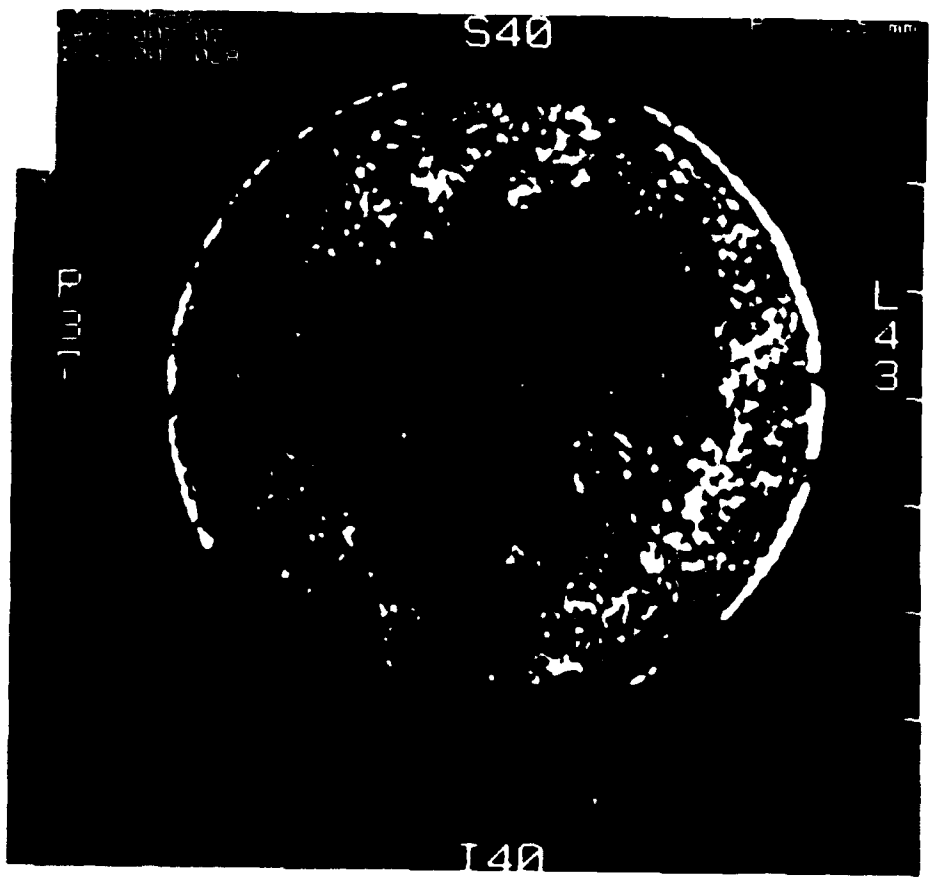
S40
I40

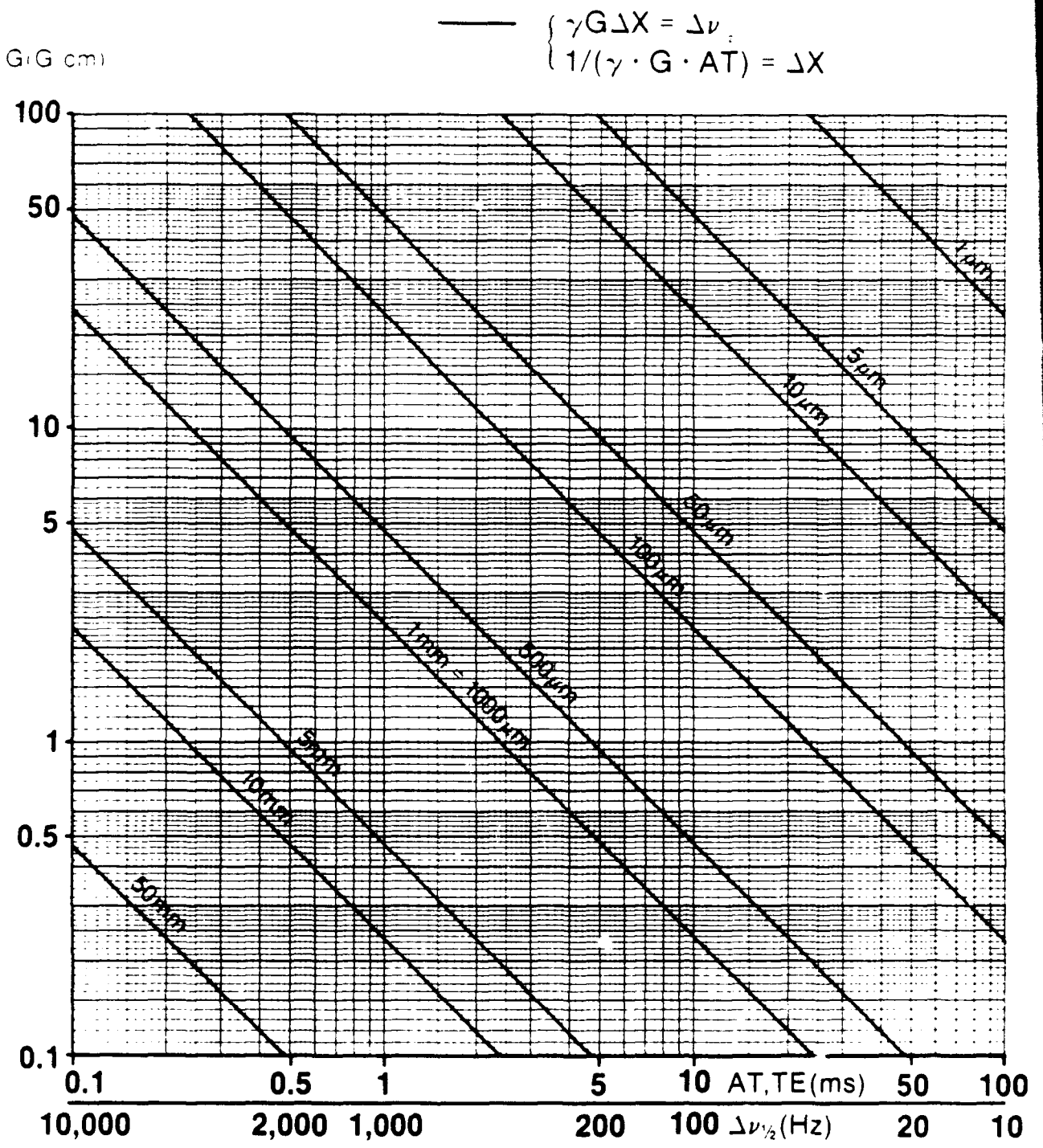
G (G cm)
$\gamma G \Delta X = \Delta \nu$
$1/(\gamma \cdot G \cdot AT) = \Delta X$
100
50
10
5
1
0.5
0.1
1 μm
5 μm
10 μm
50 μm
100 μm
500 μm
1mm ~ 1000 μm
5mm
10mm
50mm
0.1
0.5
1
5
10
AT, TE (ms)
50
100
10,000
2,000
1,000
200
100
$\Delta \nu_{1/2}$ (Hz)
20
10

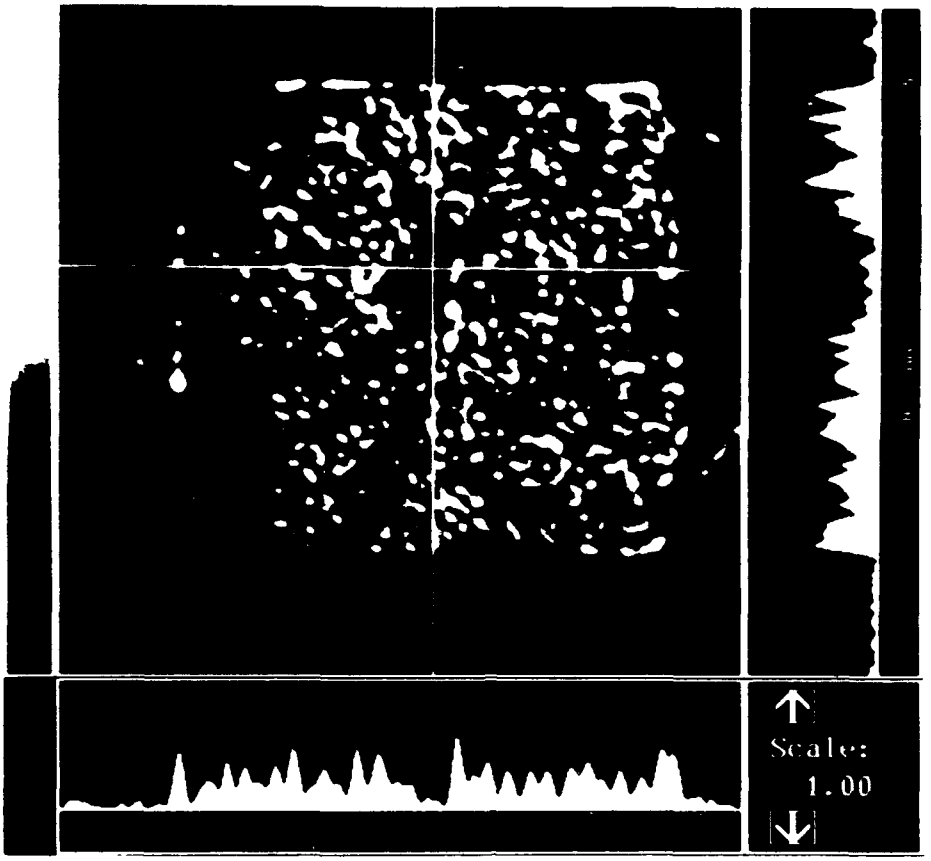
Scale:
1.00

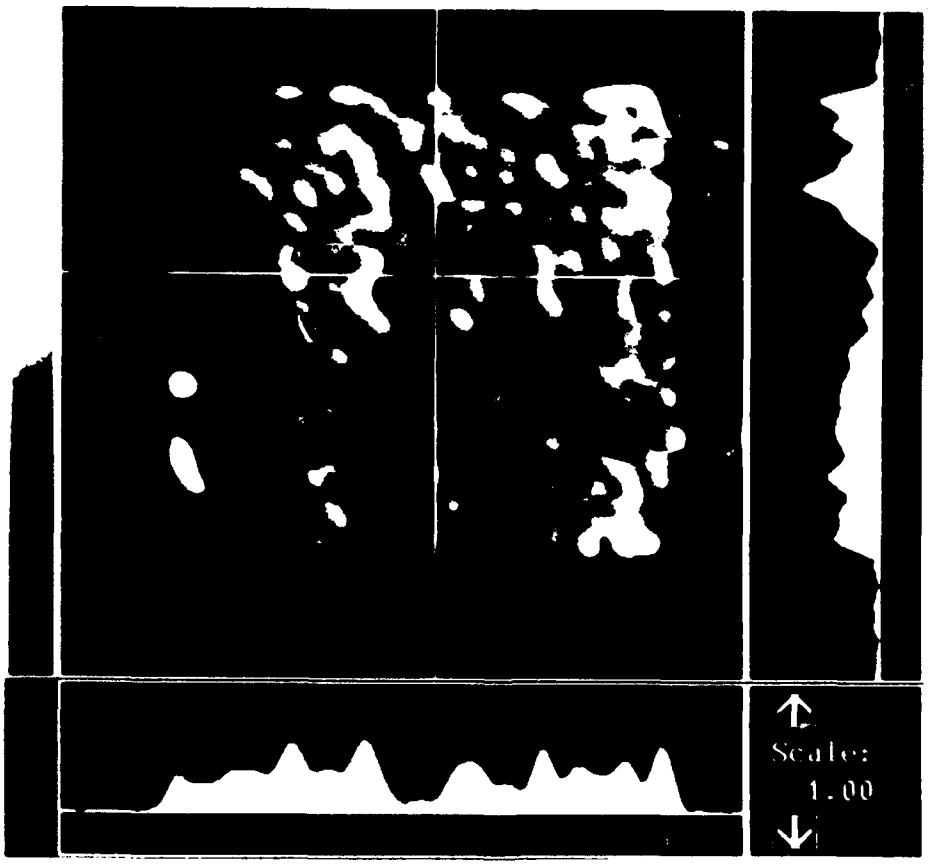
Scale:
1.00

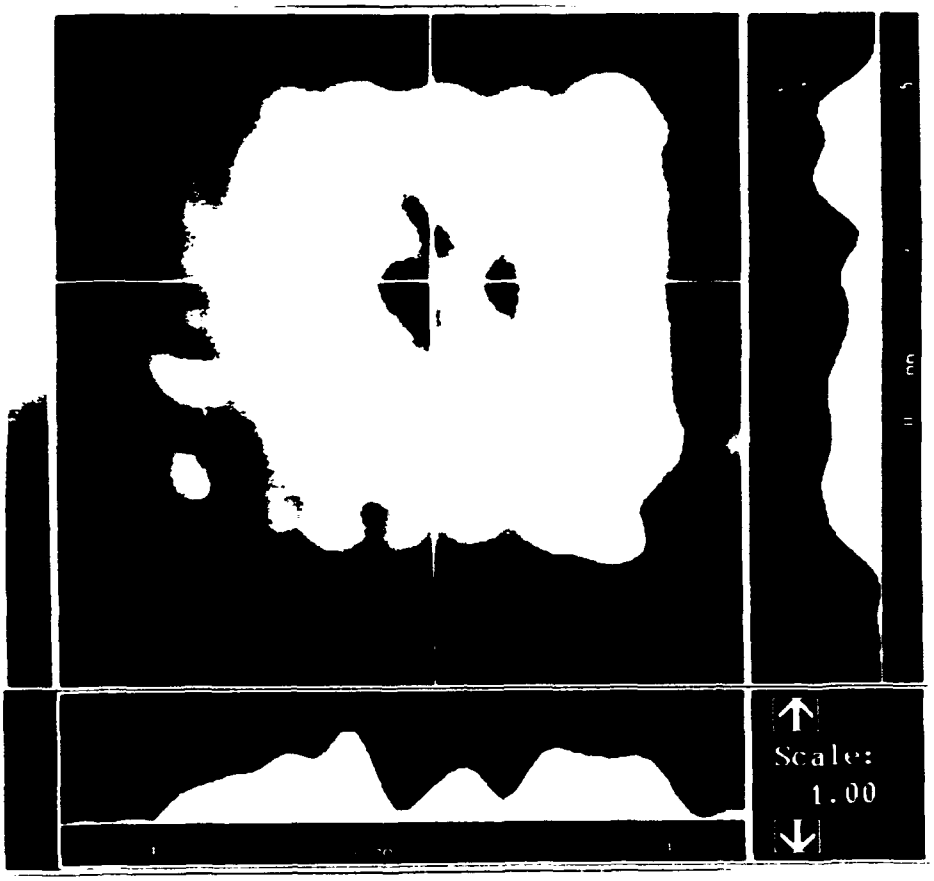
Scale:
1.00

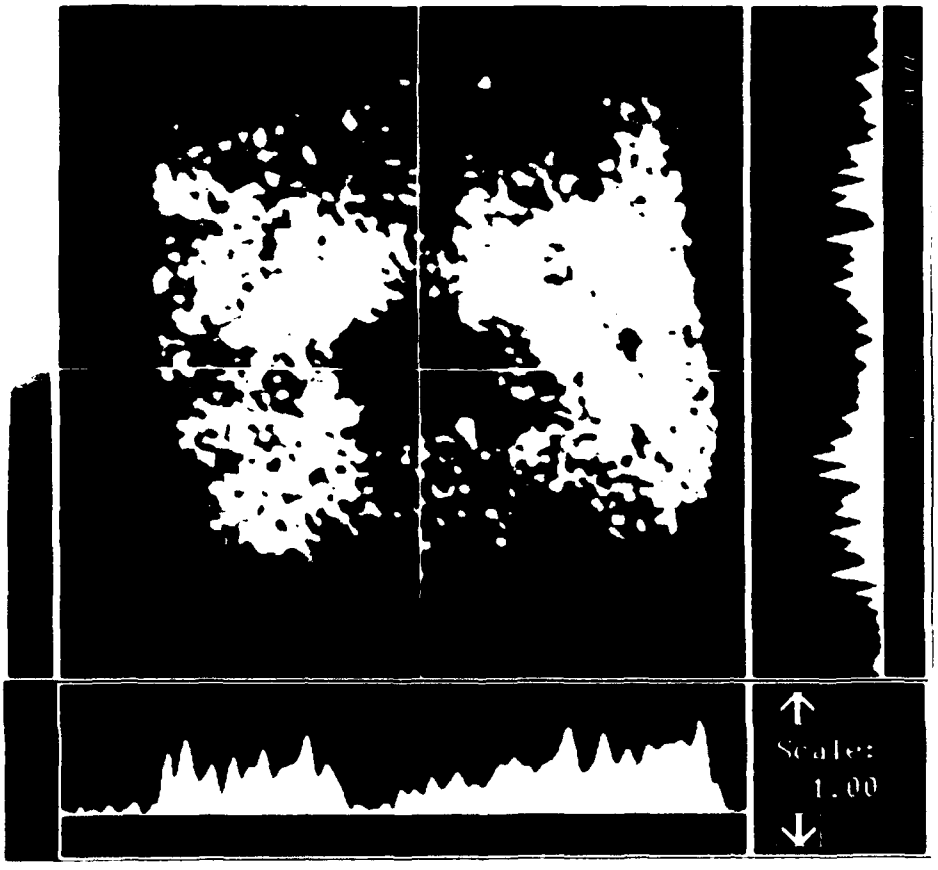
Scale:
1.00

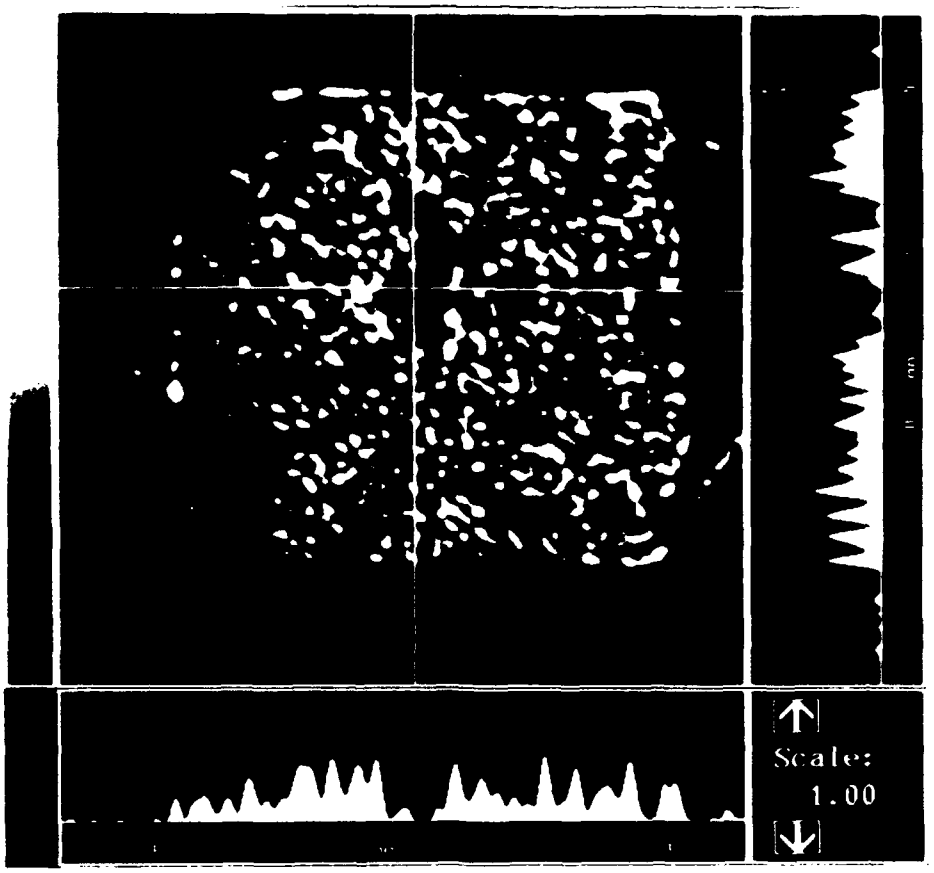
Scale:
1.00

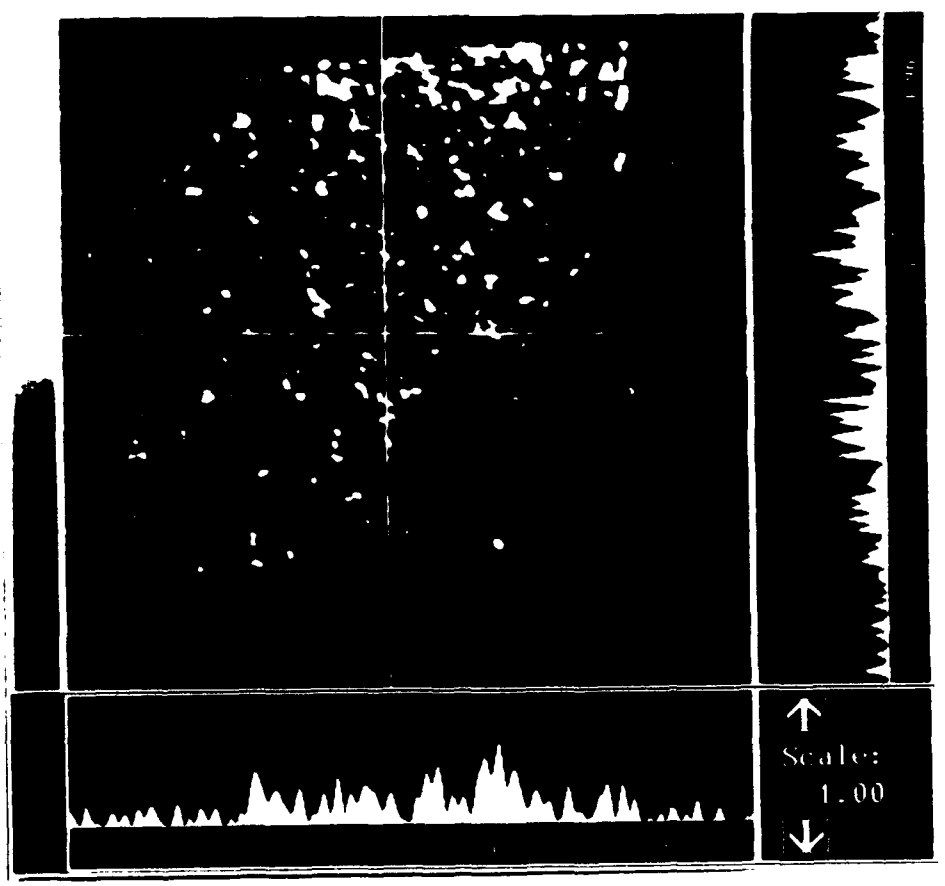
Scale:
1.00

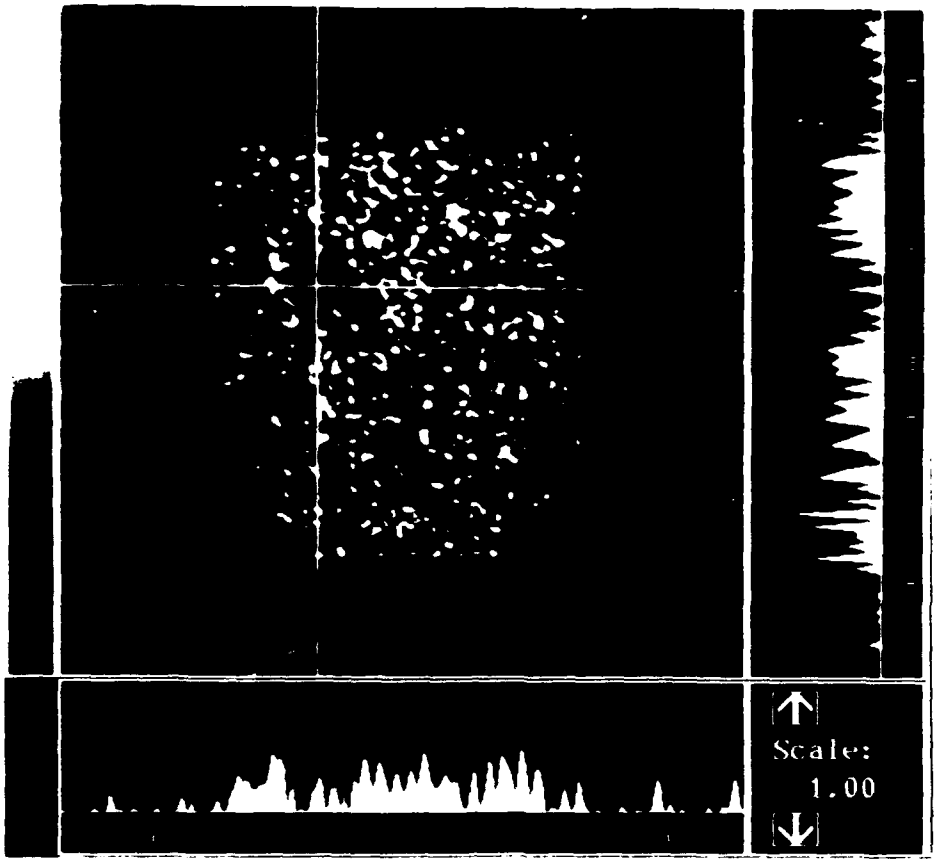
Scale:
1.00

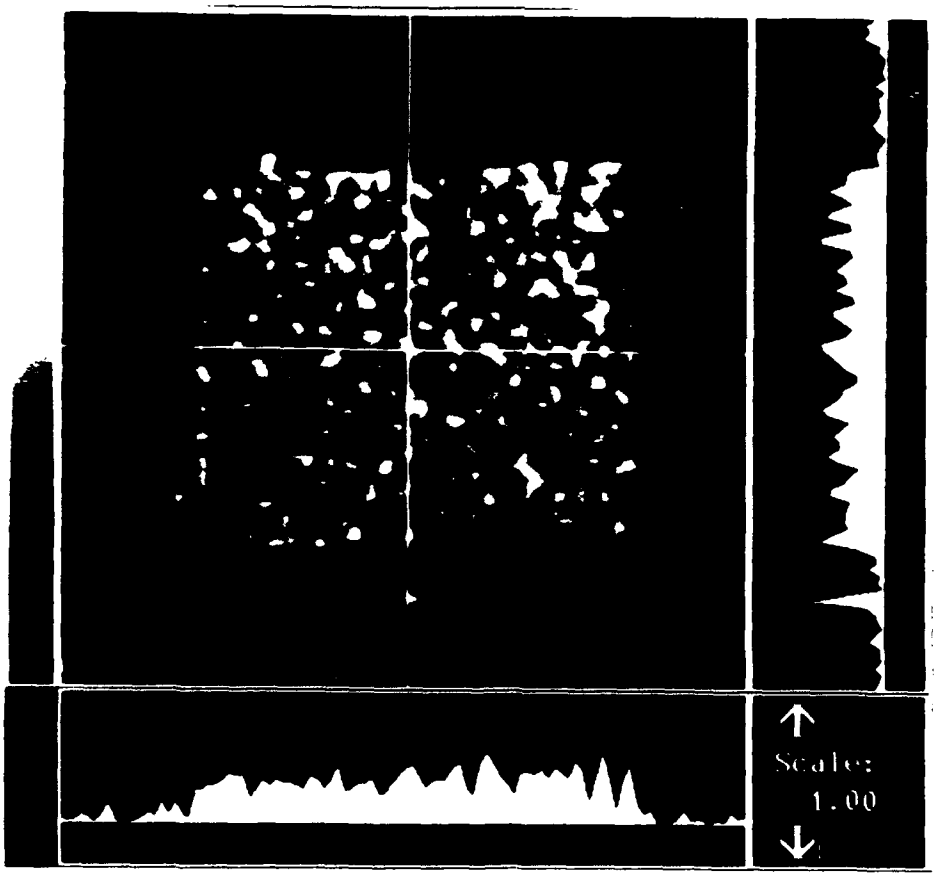
Scale:
1.00

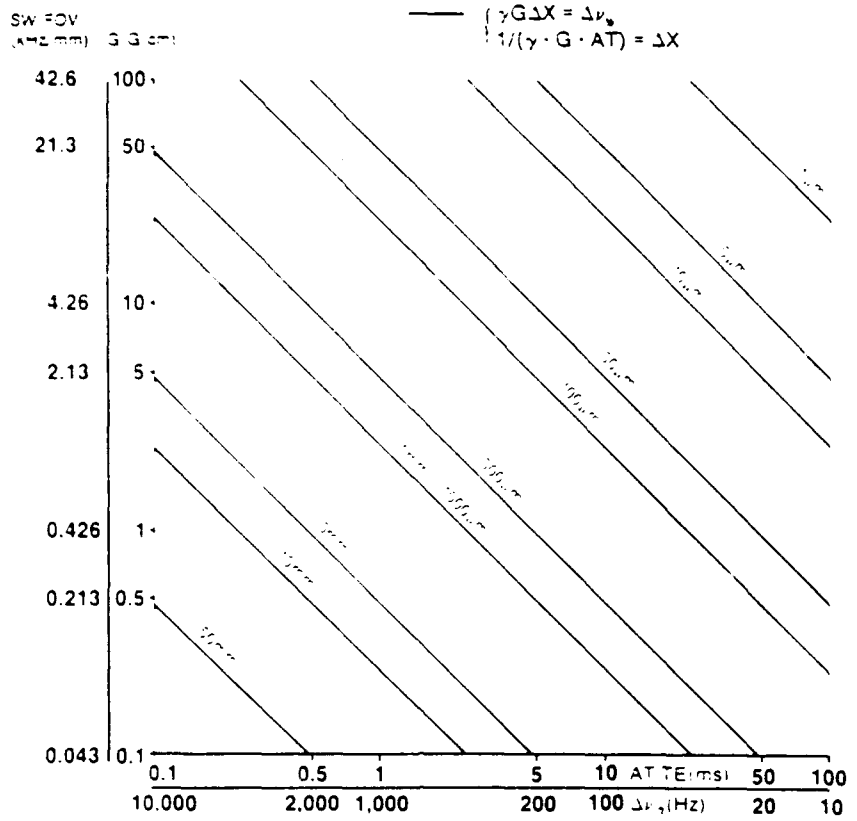

Figure 1. Plots of G and spectral width (SW)/field of view (FOV) versus AT (TE) or line width for various resolutions.

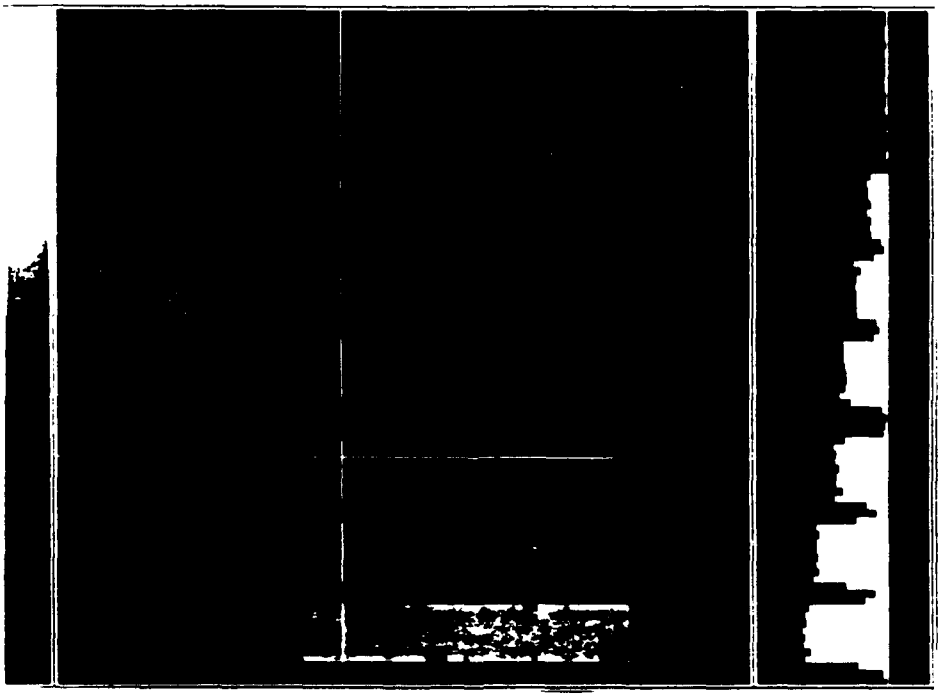

Figure 2. NMR image of a series of 2-mm sheets of cured, filled CB/SBR blends. Polymer compositions (CB:SBR) are from bottom: 100:0, 80:20, 60:40, 40:60, 20:80, 0:100.

NMR IMAGING OF ELASTOMERS AND POROUS MEDIA

RICHARD A. KOMOROSKI AND SUBHENDRA N. SARKAR
University of Arkansas for Medical Sciences, Departments of Radiology and Pathology, 4301 West Markham St., Little Rock, AR 72205.

ABSTRACT

NMR imaging has been applied to some elastomeric materials of industrial interest. The T_2s of common elastomers, particularly after filling and curing, are sufficiently short that spin-echo sequences at submillisecond echo times cannot produce T_2-independent images. The sensitivity to T_2 potentially makes spin echo imaging a good probe of elastomer blend composition, as demonstrated for a series of filled and cured cis-polybutadiene, styrene-butadiene rubber blends. The technique can be used to distinguish good and bad carbon black dispersion in actual tire tread samples. The configuration of polyester tire cord, voids, rubber layer boundaries, apparent migration of additives, and other inhomogeneities can be detected in end-product tire samples. The value of isotropic voxels at 80-100 um and the effect of resolution relative to pore size are demonstrated on a model, H_2O-saturated porous glass disk of 200-um average pore size. The feasibility of multinuclear NMR imaging for fluid-specific characterization of porous materials such as oil cores is demonstrated for ^7Li and ^{19}F.

INTRODUCTION

Nuclear magnetic resonance (NMR) imaging is being vigorously pursued as a nondestructive characterization tool for materials. The promise of measuring spin concentration, molecular mobility [via the spin-lattice (T_1) and spin-spin (T_2) relaxation times], and chemical structure (by largely unrealized localized spectroscopy techniques) at various locations within a sample has resulted in initial applications in a wide variety of nonmedical areas.[1] Sizes have ranged from tree trunks of 25-cm diameter [2] to "microscopic" studies on millimeter-sized objects at 50-100 um resolution.[3,4]

Because standard NMR imaging techniques are limited to observing molecularly mobile components, applications to date have concentrated on bulk elastomers [5], solvent diffusion [6], and liquids in porous inorganic materials such as ceramics and oil cores.[7,8] Techniques are being developed for imaging of highly rigid materials [9], which is the subject of other papers in this proceedings.

For standard NMR imaging techniques, the primary requirement for increased resolution is powerful gradients. For medical imaging, gradients typically never exceed 1 G/cm. Figure 1 shows plots of gradient strength G vs. acquisition time AT for various image resolutions. The significance of the acquisition time is that in echo imaging, it is limited by (and often equal to) the echo time TE. For materials, T_2 can be quite short, and hence TE or AT cannot be lengthened without

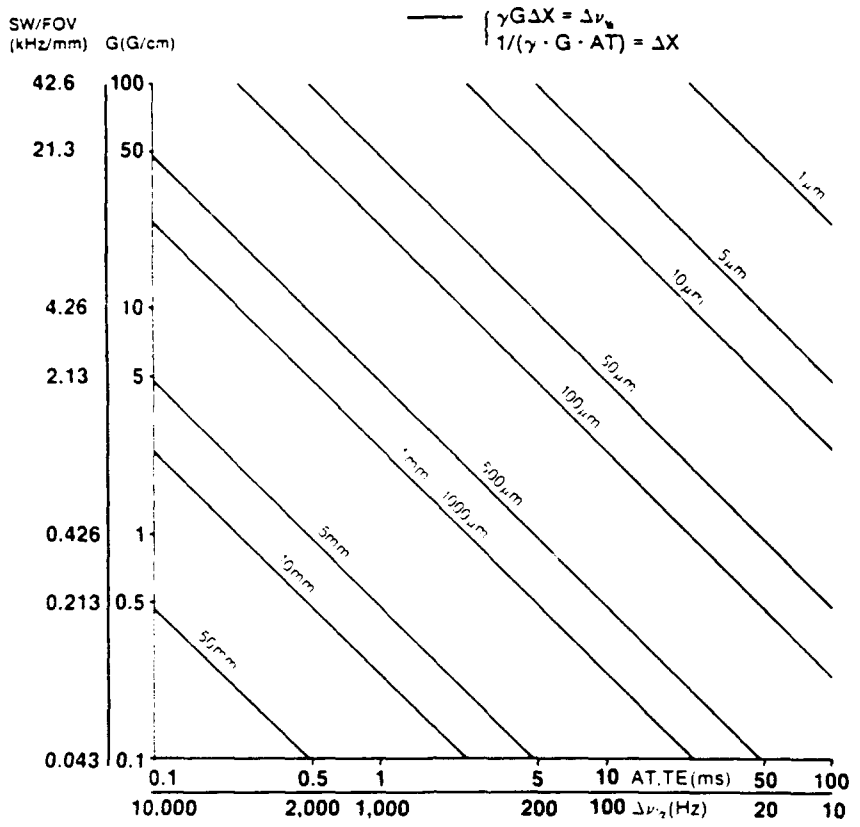

Figure 1. Plots of G and spectral width (SW)/field of view (FOV) versus AT (TE) or line width for various resolutions.

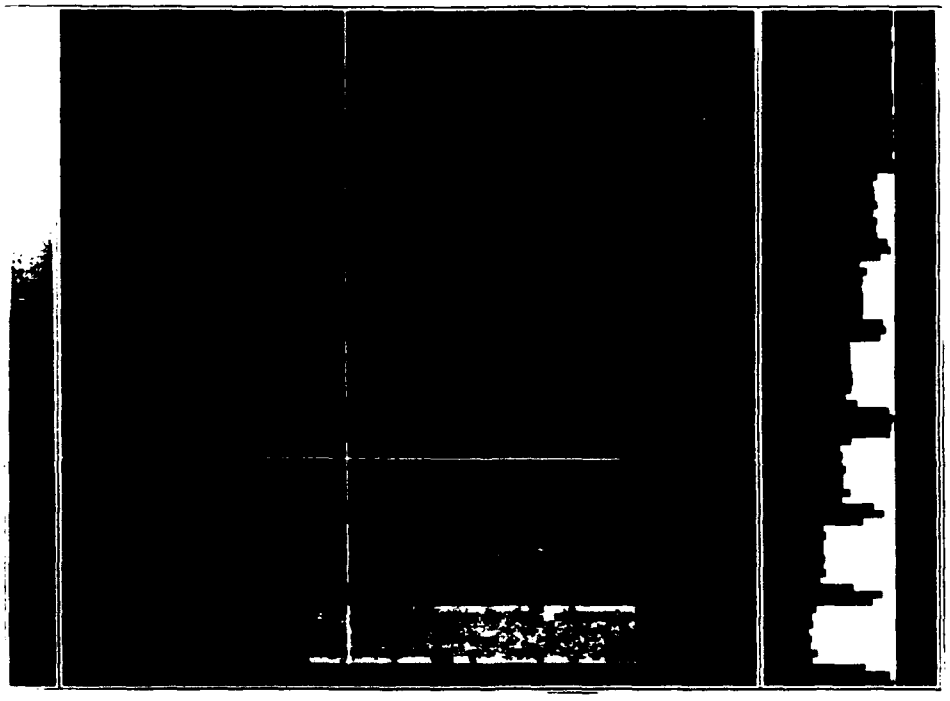

Figure 2. NMR image of a series of 2-mm sheets of cured, filled CB/SBR blends. Polymer compositions (CB:SBR) are from bottom: 100:0, 80:20, 60:40, 40:60, 20:80, 0:100.

loss of echo signal. Another consideration is the resonance line width of the material. The spread of frequencies caused by the gradient must be larger than the spread inherent in the line width. This relationship is also shown in Figure 1 for the limiting case where gradient spread equals the line width. Hence the relatively large line widths seen for materials also necessitate powerful gradients, typically 10 G/cm or larger.

In this report we explore applications of NMR imaging to direct analysis of bulk elastomeric materials of industrial interest and porous media. Current limitations and new directions of research are discussed.

EXPERIMENTAL METHODS

The ^{1}H NMR images were acquired at 200.1 MHz on a General Electric Omega CSI-4.7 system with Acustar shielded gradients and available bore size of 120 mm. The maximum gradient strength was 20 G/cm. Either a standard single-plane, spin-echo sequence with slice-selective 90 and 180° pulses [5] or a 3D volume imaging sequence was used. The 3D volume sequence employed a hard, initial 90° excitation pulse of 15-70 us (depending on the coil) to excite spins in the entire object. Phase encoding was performed in the slice-select direction and one transverse direction, with frequency encoding in the remaining direction. For small objects at higher resolution, a commercial, single-turn surface coil of 2-cm diameter was used for both excitation and detection. For larger objects and oil cores, a 6.0-cm diameter, home-made birdcage coil was used. Lithium-7 and ^{19}F images were acquired on the same instrument at 77.8 and 188.2 MHz, respectively. For ^{7}Li a 5.5-cm birdcage coil was used, whereas for ^{19}F a 2-cm, single-turn surface coil provided both excitation and detection.

Carbon-13 NMR spectra were acquired at 75 MHz and 90°C on a General Electric GN-300 WB high resolution spectrometer with proton scalar decoupling in spinning 10-mm NMR tubes.

RESULTS AND DISCUSSION

Elastomer Composition and T_2

We previously demonstrated that standard spin-echo techniques at TEs of 10 ms or greater could be used successfully to image favorable cases of cured elastomers.[5] Many common elastomers have T_2s of 0.5-2 ms [10], making it necessary to use short TE sequences such as 3D volume imaging described above to capture sufficient signal intensity. We have imaged elastomeric materials at TEs as low as 500 us. However, even at submillisecond TEs it is not possible to obtain images for typical pure elastomers without T_2 affecting signal intensity and contrast. Of course, the filling and curing that impart the desired mechanical properties further reduce T_2 from that of the pure elastomer.

Figure 2 shows an NMR image (200 x 200 x 500 um voxels) from a 3D volume dataset for a phantom composed of 2-mm sheets of a common series of cured, carbon-black filled cis-polybutadiene, emulsion styrene-butadiene rubber (CB/SBR) blends. Although all the blends have approximately the same hydrogen content, image intensity varies dramatically among the

blends. As the S. (T_g = -70°C) content inc. ases relative to CB (T_g = -102°C), T_2 decreases and image intensity decreases at a TE of 1.2 ms, as in Figure 2, or even at a TE of 500 us. This is also apparent from the image profile on the right in Figure 2.

Conversely, the results in Figure 2 illustrate that NMR imaging can be a sensitive measure of polymer blend composition in well defined situations. Differences as small as 10% may be detectable. Such an approach may provide a substitute for localized spectroscopy techniques, which currently seem of limited use for complex, short T_2 materials.

Tire Materials

Inhomogeneities in elastomers have been imaged directly [5,11] and by solvent swelling.[12] Detection of an ^{1}H-rich, relatively mobile swelling agent in a polymeric material produces images of high quality. However, spatially dependent differential swelling and dimensional changes make interpretation of such images problematic. Direct imaging at short TE of cured, filled elastomer blends such as tire sections is preferred and can be highly informative. Figure 3 shows NMR images (250 x 250 x 500 um voxels, TE = 4 ms) of actual finished tire tread sections. The section in Figure 3A was from a tire tread with a good, homogeneous carbon black dispersion, whereas that in Figure 3B had a poor dispersion. The samples appeared visually similar. The images are dramatically different and reflect the degree of filler dispersion. The good dispersion image has a relatively even distribution of NMR intensity, whereas the poor dispersion image appears spotty and highly heterogeneous, even in higher resolution (200^3 um^3) images of thinner slices throughout the sample. Tread grooves are seen in both images. Numerous local inhomogeneities of a lesser nature are also seen in Figure 3A. We have routinely observed such inhomogeneties in a variety of elastomer compounds, both cured and uncured.

Figure 4 is an NMR image (100 x 100 x 200 um voxels at TE of 2 ms) of a transverse section of a simple tire containing polyester fiber tire cord. The arrangement and shape of the cord fibers, as well as numerous irregularities, are clearly visible. The laminate structure of the section is well defined. This consists of a 2-mm wide layer on the left which corresponds to the tread. This is bonded to the 5.5 mm layer containing the cords in the center, with a barely visible 2-mm layer on the right. The right-hand layer is the inner liner of the tire, and it appears to consist of two layers from the image and profile although visually this is not apparent.

Carbon-13 NMR spectra of samples taken from the left (closest to the cord) and right sides of the right hand layer show the elastomeric components of these to consist of an isoprene rubber, butyl rubber blend, and probably pure butyl rubber, respectively. This is not unexpected as butyl rubber is commonly used as an air barrier on the inner surface of tubeless tires. It also explains the difficulty in observing this layer by NMR imaging. Butyl rubber is very difficult to image by standard techniques [5] because of its uncharacteristically short T_2, which is a consequence of reduced chain segmental mobility.[13] The addition of isoprene rubber to butyl would increase segmental mobility in the blend, making that layer more

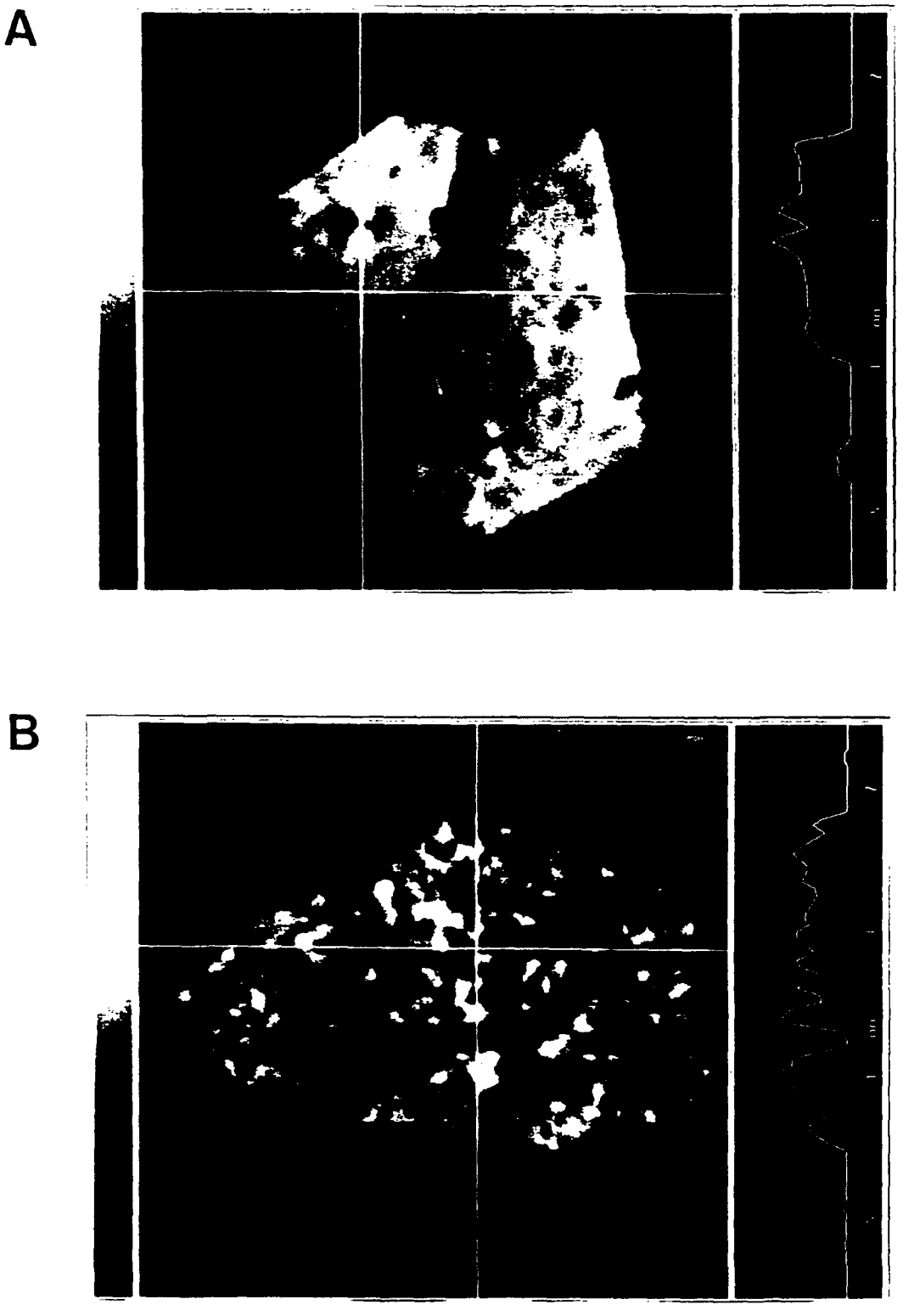

Figure 3. NMR images of actual finished tire tread sections. Tread grooves are seen in each image. A) Good dispersion of carbon black; B) bad dispersion of carbon black. TE = 4 ms. 250 x 250 x 500 mm voxels.

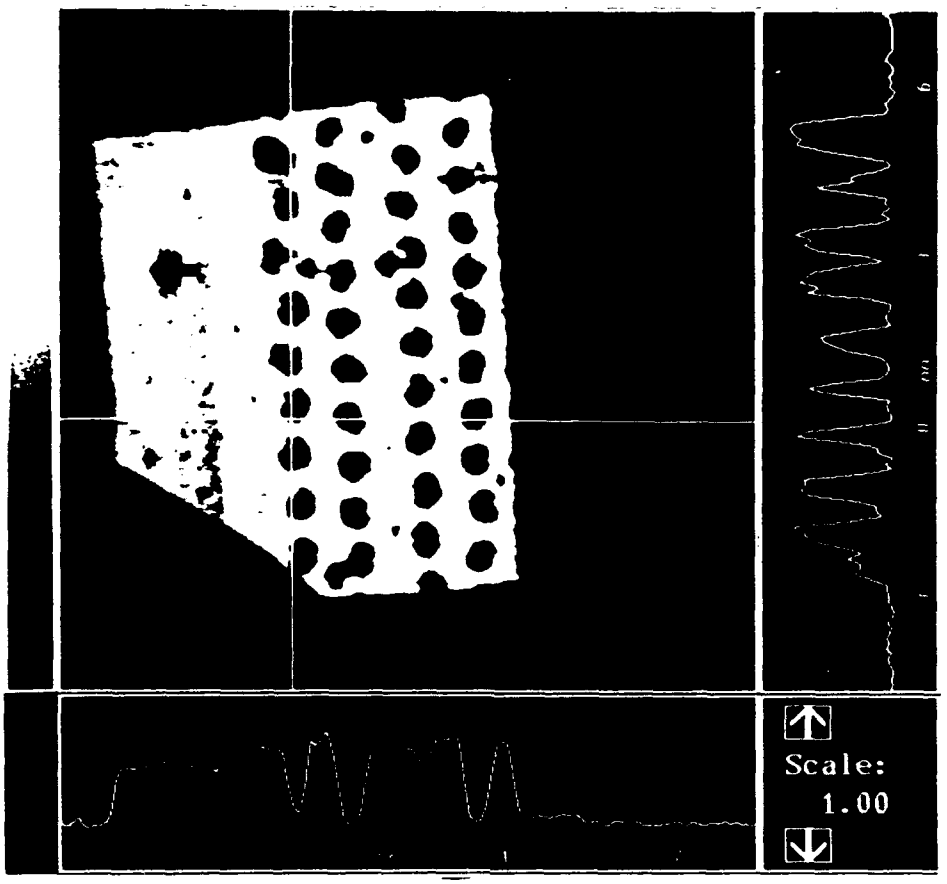

Figure 4. NMR image (slice #9 of 16, 100 x 100 x 200 um voxels, TE = 2 ms) of a tire section with polyester cord belts. The FOV is 12.8 x 12.8 mm. One two-component layer, due to the inner liner of the tire, is barely visible on the right side of the image.

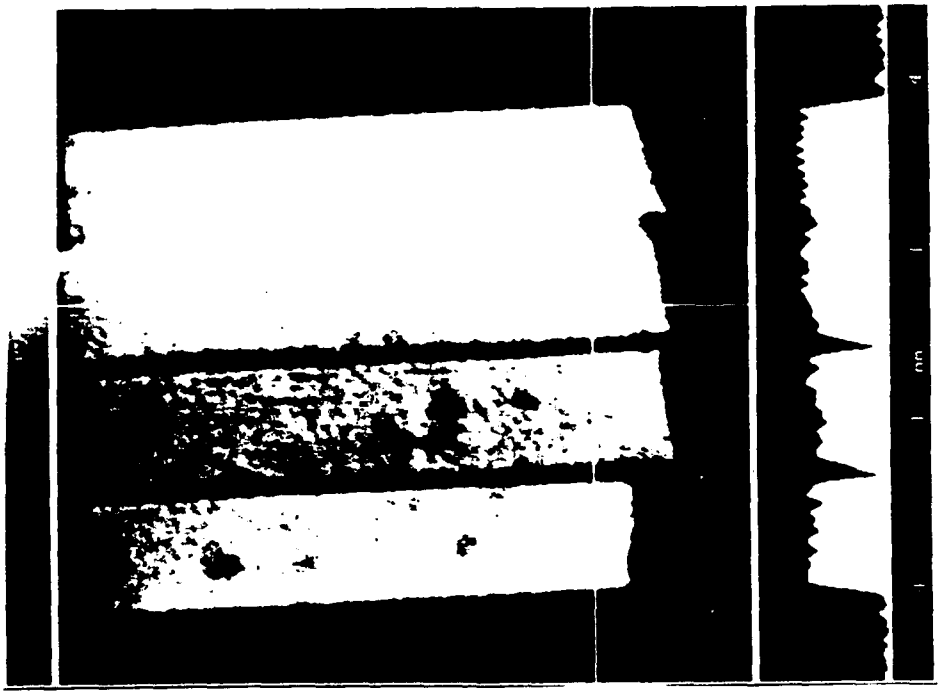

Figure 5. Image (80 x 80 x 500 um voxels, TE = 4.3 ms) of 4 cured, filled 2-mm CB sheets. The bottom three sheets are separated by glass spacers of 180-um thickness. The top two sheets have no spacer.

visible than pure butyl in the image. This sample has a material feature that might have gone undetected without NMR imaging.

The relatively large feature in the left layer consists of a low-intensity region surrounded by three spots of higher intensity. This is apparently a solid particle or void with adjacent, small areas of unknown origin. We speculate that these may be some combination of a) regions of higher rubber, lower filler content and normal cure; b) undercured regions; or c) regions to which low molecular weight additives have migrated, producing either increased polymer mobility or contributing signal intensity directly to the image.

In the image in Figure 4 the rubber layer boundaries are well defined because the layers have different combinations of T_2 and mobile hydrogen densities. For layers of identical material, detection of layer boundaries may be less straightforward. We previously demonstrated that in model elastomers boundaries beyond the image resolution can be detected by reduction of voxel intensity at that point.[5] Under the relatively poor resolution and long TE conditions of the previously published images [5], it was not clear if such sub-resolution boundary detection was from depletion of hydrogen content, lower T_2 at the surface, or both. Figure 5 shows higher resolution (80 x 80 x 500 um) images of the same sheets as before [5] with 180-um spacers at two boundaries and with no spacer at the third boundary. The sheets were firmly pressed together and secured for this experiment to eliminate the possibility of casual air space between the sheets. As expected, the spacers were well resolved. However, the boundary without spacer was also detected. Examination of image profiles at higher resolution suggests that this arises (under these conditions) from a slightly reduced amount of NMR visible rubber in the 200-um region at the surface of the sheet. Hahn spin-echo experiments between 3 and 10 ms measure essentially the same T_2 at the surface as in the bulk rubber.[10] These results suggest that laminate boundaries may be more readily detectable for separately cured sheets than for uncured or co-cured materials.

Model Porous Materials

To date, most NMR imaging of materials has been with highly anisotropic voxels and poor resolution perpendicular to the slice. The advantage of isotropic voxels for visualizing complex 3D structures and minimizing confusing partial volume effects has been recognized.[14] Although 3D volume imaging may ultimately be the method of choice for obtaining isotropic voxels, it is possible to use the single-slice technique at moderately good resolution. Figures 6A-C show images of a 7 x 7 mm piece of a water-saturated, porous glass disk (35% porosity, pore size 170-220 um) at three different isotropic resolutions-less than, at, and greater than the nominal pore size. As expected, the images are dramatically different and, in particular, display how features in the low resolution image arise from different planes in the slice. In the 100-um isotropic-voxel image, there are a few small and intense spots whose size is about 190 um x 190 um in plane and are either single pores or collections of smaller pores. Longer spots may be pores connected in plane. Small and weak spots may be from

A

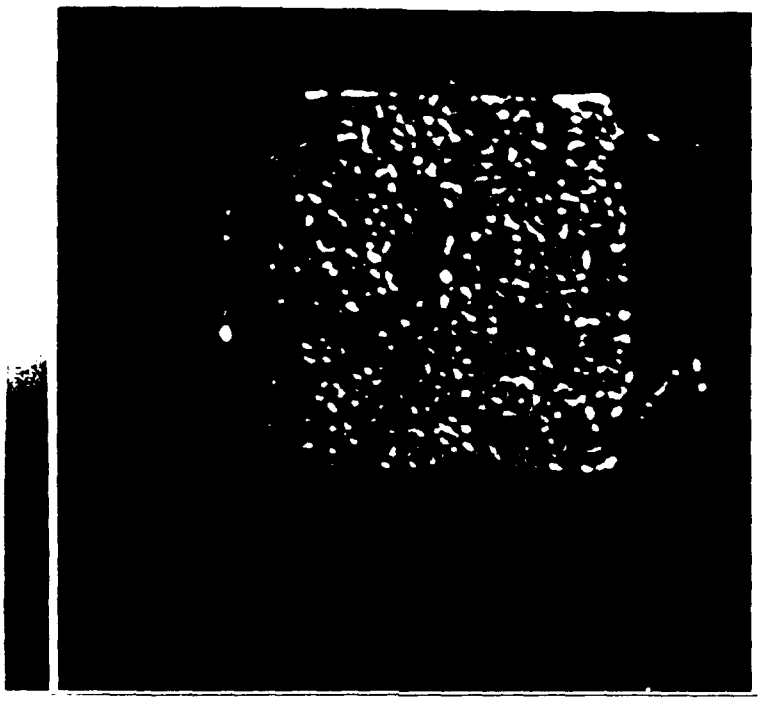

B

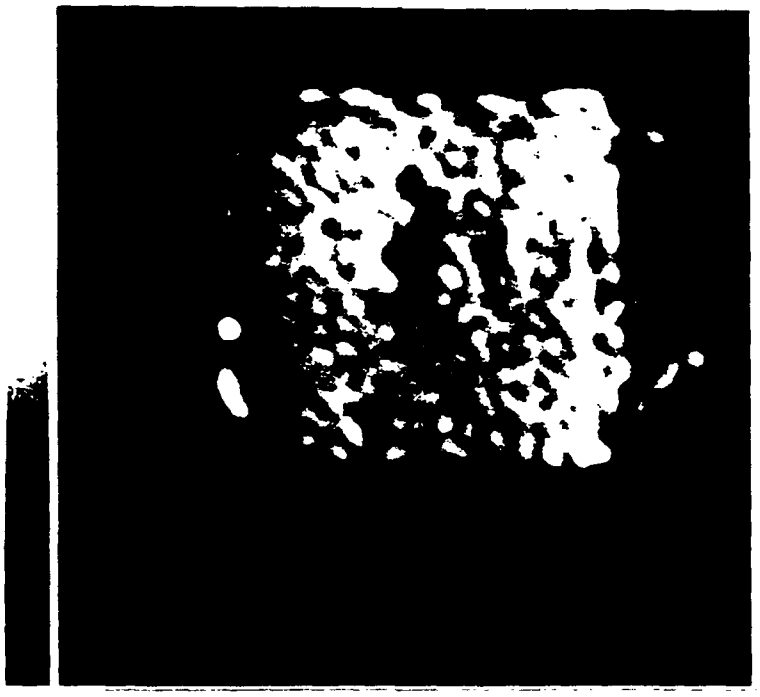

C

D

Figure 6. NMR images of a 7 x 7 mm portion of a sintered glass disk of 35% porosity and nominal pore size 170-220 um at three isotropic resolutions: A) 100 um; B) 200 um; and C) 400 um; D) 100 x 100 x 2000 um voxels.

pores of about 10 um size or less and fully included in the slice, or from larger pores partially cut by the 100-um slice. For the 200-um and 400-um isotropic resolution images (Figures 6B and 6C, respectively), a few intense spots become larger as the resolution becomes coarser. Some of the spots remain bright, implying perhaps collections of water-filled pores from various planes. Images of other porous glass disks of 5-50 um pore size suggest that the image appearance is dominated by the large-pore tail of a pore size distribution.[10]

The higher-resolution appearance of Figure 6A is retained to some extent in Figure 6D, an image with 100 x 100 x 2000 um voxels, even though features from the equivalent of twenty 100-um slice thicknesses contribute to the latter image. This arises from the fact that the majority of the object volume in this case is occupied by glass or air, and hence many of the anisotropic voxels have little or no signal. For porous materials of low-to-medium porosity and relatively large pore size, thick slices may provide more useful information than for relatively homogeneous materials such as polymers.

The results of Figure 6 also demonstrate that obtaining isotropic voxels at high resolution will not exact too severe a penalty in S/N ratio for porous materials. Although the voxel volume in the 100-um image is 1/64th that of the 400-um image, it took only 16 times (4x S/N penalty) as long to obtain the 100-um image. This arises from the "dilution" of the signal in a single voxel by glass as the resolution becomes coarser.

Multinuclear Imaging of Porous Materials

NMR imaging is being used increasingly to study the fluid distribution in oil cores.[8,15] Since such imaging is usually concerned with the distribution of two or more fluids such as oil and water in the rock, methods for separate observation of the components must be developed. For cases where individual resonances can be resolved for the oil and water components, we have used a radiofrequency presaturation pulse and dephasing gradient to produce component-selective images.[15] When resonance lines are broad and the individual components cannot be resolved, a multinuclear approach is necessary. Edelstein et al. [8] have used the ^{1}H and ^{13}C isotopes to analyze for the amounts of water and oil in whole cores. We have indirectly imaged a third fluid (isopropanol as a model miscible injectant) in a core by profiling the disappearance of signal in the ^{1}H NMR image when the third fluid is deuterated.[15]

Direct multinuclear imaging of isotopes confined to a single phase should provide unambiguous separation of two or more components in model systems. Possible nuclei include ^{19}F (fluoride or fluorinated organics), ^{13}C (organics, CO_2), ^{23}Na (brine), ^{7}Li (brine), ^{2}D (D_2O or deuterated organics), and ^{17}O (H_2O), in addition to ^{1}H. As an example, Figure 7A shows the ^{7}Li NMR image of a Li brine in a model porous glass filter disk of nominal pore size of 200 um. The ^{7}Li isotope is favorable for such studies, with a sensitivity about 27% that of ^{1}H, relatively narrow lines, T_2s of 10-500 ms, and T_1s of 0.5-4 s in motionally restricted systems. Figure 7A shows that a resolution on the order of 1 x 1 x 5 mm^3 can be expected. Figure 7B shows a comparable image for ^{19}F of 50% hexafluorobenzene in porous glass taken using a surface coil. We have obtained preliminary ^{7}Li and ^{19}F images on actual oil cores.

Kumovski Page 10 of 12

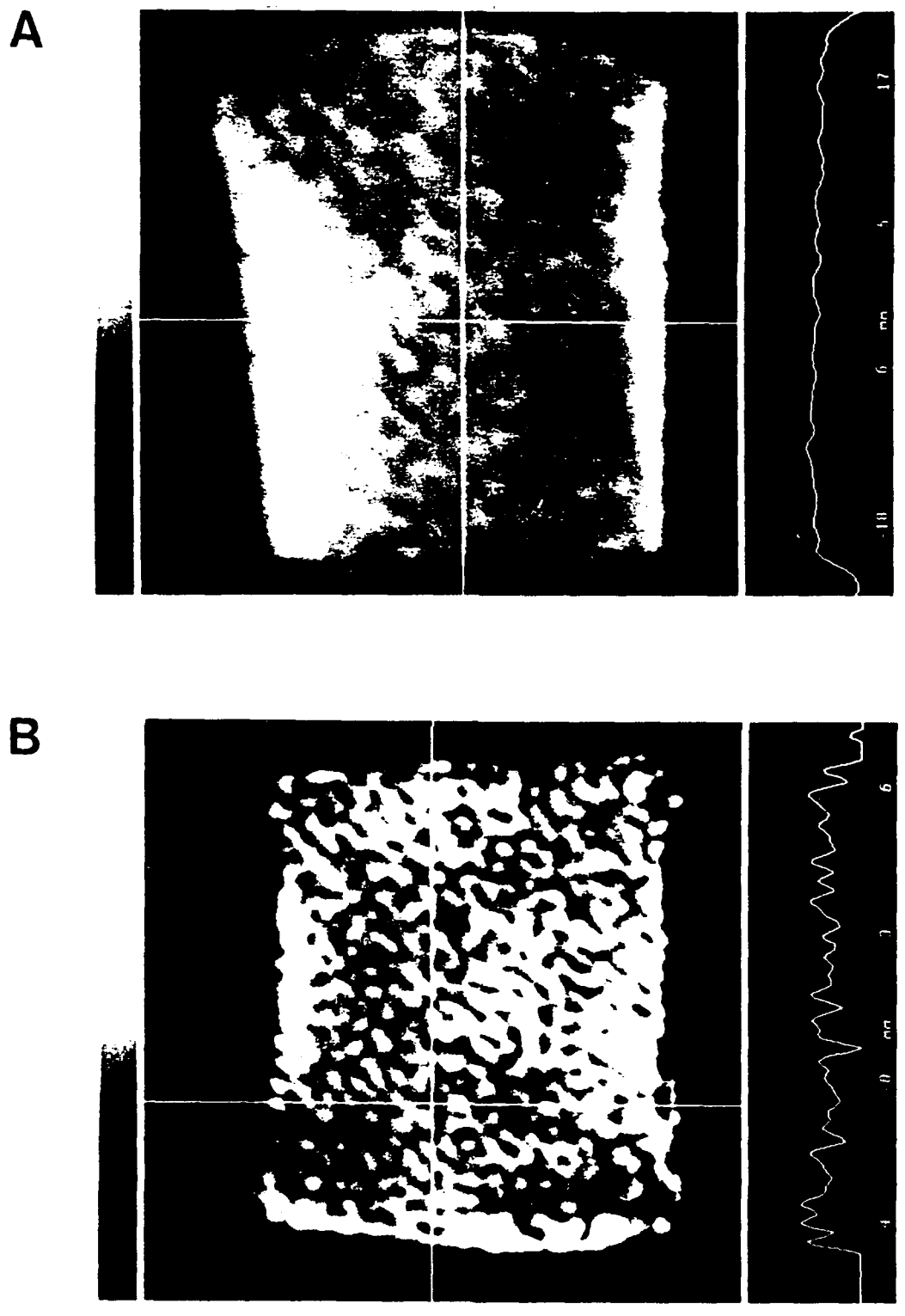

Figure 7. A) ^{7}Li NMR image of a portion of a sintered glass disk (35% porosity, 170-220 um pore size) with 2 M LiCl. (1 x 1 x 5 mm voxels; TE = 2 ms; FOV, 64 x 64 mm) B) ^{19}F NMR image of a sintered glass disk (40% porosity, 4-5.5 um pore size) with 50% hexafluorobenzene. (200 x 200 x 2000 um voxels; TE = 2.8 ms; FOV, 12.8 x 12.8 mm)

Resolution better than ^{7}Li can be expected for ^{19}F in comparable cases (Figure 7B). The ^{19}F T_2 may be short, on the order of 2 to 10 ms. For both ^{7}Li and ^{19}F it will be necessary to use short TE sequences such as whole-core 3D volume imaging.

ACKNOWLEDGEMENTS

We thank Ken Schur of the BF Goodrich Company for providing the elastomer and tire samples, and Annadell Fowler for running the ^{13}C NMR spectra. This work was supported in part by grant AFOSR-89-0418 from the Air Force Office of Scientific Research.

REFERENCES

1. J.M. Listerud, S.W. Sinton, and G.P. Drobny, Anal. Chem. 61, 23A (1989).

2. S.J. Chang, J.R. Olson, and P.C. Wang, For. Prod. J. 39, 43 (1989).

3. C.F. Jenner, Y. Xia, C.D. Eccles, and P.T. Callaghan, Nature 336, 399 (1988).

4. W. Kuhn, Angew. Chem. Int. Ed. Eng. 29, 1 (1990).

5. C. Chang and R.A. Komoroski, Macromolecules 22, 600 (1989).

6. L.A. Weisenberger and J.L. Koenig, Appl. Spectrosc. 43, 1117 (1989).

7. L. Garrido, J.L. Ackerman, and W.A. Ellingson, J. Magn. Reson. 88, 340 (1990).

8. W.A. Edelstein, H.J. Vinegar, P.N. Tutunjian, P.B. Roemer, and O.M. Mueller, SPE Paper 18272, 63rd Annual Technical Conference and Exhibition, Houston, TX, Oct. 2-5, 1988.

9. D.G. Cory, J.B. Miller, R. Turner, and A.N. Garroway, Mol. Phys. 70, 331 (1990).

10. S.N. Sarkar and R.A. Komoroski, unpublished results.

11. A.G. Webb, P. Jezzard, L.D. Hall, and S. Ng, Polym. Commun. 30, 363 (1989).

12. R.S. Clough and J.L. Koenig, J. Polym. Sci. Polym. Lett. 27, 451 (1989).

13. R.A. Komoroski and L. Mandelkern, J. Polym. Sci. Polym. Symp. 54, 201 (1976).

14. X. Zhou, C.S. Potter, P.C. Lauterbur, and B. Voth, Abstracts, Eighth Annual Meeting, Soc. Magn. Reson. Med., 286 (1989).

15. J.J. Dechter, R.A. Komoroski, and S. Ramaprasad, Proc. Soc. Core Analysts, paper #8903, 1989.